



# An experimental study of FDM parameter effects on ABS surface quality: roughness analysis

Khaoula Ouazzani<sup>1</sup> · Mostapha El Jai<sup>1,2</sup> · Iatimad Akhrif<sup>2</sup> · Mohammed Radouani<sup>1</sup> · Benaissa El Fahime<sup>1</sup>

Received: 12 March 2023 / Accepted: 11 April 2023 / Published online: 9 May 2023  
© The Author(s), under exclusive licence to Springer-Verlag London Ltd., part of Springer Nature 2023

## Abstract

Fused deposition modelling has become one of the most popular extrusion additive manufacturing technologies over the last decades, since it is easy to handle and user-friendly. However, it still requires special attention regarding its position within different industrial applications; one of the major issues that require additional improvement corresponds to the surface quality. Hence, this work is dedicated to the understanding of the roughness according to three process parameters, namely, printing speed (Spd), layer thickness (Lth), and extrusion temperature (Temp). A Taguchi L27 orthogonal-array was adopted in order to conduct this investigation. Neither post-surface treatments nor any additional surface finishing were applied. Altisurf apparatus was utilized to build 3D images and 2D profiles of the samples' peaks and depths leading to significant surface sampling regarding the statistical analysis that follows. From a quantitative standpoint, the arithmetic roughness Ra ranged between 7.18 and 13.4  $\mu\text{m}$ , while the best surface quality was reached at the higher scan speed, 4000 mm/min; the smoothest surface was produced at the lowest value of the layer thickness, 0.1 mm; finally, the higher extrusion temperature is the best is the produced surfaces. Moreover, a multiway ANOVA was carried-out leading to select the most significant factors and interactions within the set of inputs. Consequently, the resulting analysis has discriminated the most influenced parameters within the following order, Lth, Spd, and the interactions Temp \* Spd, and Lth \* Temp. Future works will propose a semi-empirical method including fluid dynamics and thermodynamics involving stochastic parameters to understand roughness variability of FDM produced samples.

**Keywords** Additive manufacturing · FDM · Surface finish · Roughness · 3D imaging · ANOVA

## 1 Introduction

During the last three decades, additive manufacturing (AM) has expanded as an emerging set of manufacturing technologies which include a variety of processes base on the concept of layer-by-layer fabrication. According to ISO/ASTM 52.900, AM techniques can be clustered into different categories based on the processed materials and type of energy: “liquid state” related to extrusion processes, such as fused deposition modeling (FDM), and polymerization processes, cementitious and clay-based materials; “solid-based” consisting in lamination process; and “power-based” that includes sintering, binding,

and melting processes [1–3]. Laser beam powder bed fusion of metals (PBF-LB/M) and polymers (PBF-LB/P) [4], electron beam powder bed fusion for metals (PBF-EB/M) [5], and material extrusion-based (MEX) are the classical processes' varieties of AM that proposed by the ISO/ASTM 52.900 standards.

Concerning the FDM technology, this is one of the most used AM processes as it is user-friendly, simple in handling, and costly effective. The FDM belongs to the MEx class of AM processes as described by ISO/ASTM 52.900; it consists of a layer-by-layer extrusion of the material filament and deposition on a pre-heated bed until the final part is built. This technique is used in several fields in the form of both rapid prototyping (RP) and end-use parts. Moreover, the FDM process and its variants cover a wide range of plastics and composites as either reinforced or blends materials [6, 7].

Such as all AM processes, the FDM final products' properties are very dependable and sensitive to the processing parameters; the specialized literature has widely explored

✉ Mostapha El Jai  
m.eljai@euromed.org

<sup>1</sup> Mechanic, Mechatronic and Command Laboratory, ENSAM, Ismail University of Meknès, Meknes, Moulay, Morocco

<sup>2</sup> Euromed Center of Research, Euromed Polytechnic School, Euromed University of Fez, Fez, Morocco

the interplay between the processing parameters allowing the modeling and the understanding of the final characteristics that can be summarized according to the following list:

- Geometric and dimensional accuracy;
- Mechanical properties, such as stiffness, elasticity, dynamical behavior, choc behavior, and so forth;
- Surface properties and roughness;
- Melt behavior (Filament): die swell, bond formation, etc.

Indeed, various works were interested in the final part's characteristics; Montero et al. [8], Ahn et al. [9], and Fernandez-vicente et al. [10] studied the impact of different combinations of process parameters on ABS part properties: tensile properties, compressive strength, failure modes, and shear stress. El Jai et al. [11] investigated the compressive behavior of a new family of FDM-ABS lattice structures, while Rangisetty and Peel studied FDM products made of thermoplastic composites of ABS [12]. Further works such as Sood et al. [13] and by Alafaghani and Qattawi [14] focused on dimensional accuracy by investigating the effect of various process parameters, whereas Lieneke et al. experimentally determined both tolerance ranges and dimensional deviation of ABS parts produced by FDM [15].

From a quality standpoint, one should notice the related literature as a basis of the parameters' sensitivity analysis of the present paper. For instance, various works studied the effect of different combinations of process parameters on the surface finish. Xu et al. [16] investigated the capacity of four AM techniques, including FDM, as well as the related performance regarding surface quality and other characteristics. Anitha et al. [17] analyzed the surface roughness of FDM parts by investigating three process parameters, namely, layer thickness, deposition speed, and filament width. In addition, Byun et al. aimed to find the optimal “part orientation” to improve surface roughness

for different AM techniques — including the FDM process — [18]. Saad et al. [19] worked on enhancing the surface quality of FDM parts by finding the optimal combination of parameters through several methods. Meanwhile, other researchers worked on roughness minimization using various surface treatments (post-processing), as it is the case for Jee and Sachs which targeted the improvement the quality of additively manufactured parts [20]. As for Lalehpour et al. [21], they studied the effect of smoothing parameters on surface roughness for “acetone vapor bath” treatment. Another group of researchers worked on surface roughness of extruded parts based on theoretical and analytical models such as [22–24].

Based on the above, the end-use parts' quality involves a number of parameters that can be organized according to the Ishikawa standpoint or diagram as it is exhibited in Fig. 1. Additionally, Table 1 gathers the two-fold {Method, Machine} parameters that should impact the surface quality of the FDM-build parts.

Furthermore, it is noteworthy that other researchers characterized surface finish using classical tools as they used only a few roughness indicators and sometimes 2D profiles as a basis of comparison; this was the case in the work of Anitha et al. which adopted the arithmetic Ra as a sole indicator [17], while Thrimurthulu et al. used both formulas of Ra and 2D profiles to quantify the roughness [26]. Xu et al. worked with number of roughness indicators namely the arithmetic mean deviation “Ra,” the difference between profile highest peak and lowest valley “Rt,” and the maximum peak height relative to mean line Rpm as well as 2D surface profiles [16]. Chohan and Singh [27] carried out the same analysis to characterize the parts' surface before and after smoothing. Nevertheless, such indicators, measured on a given measurement line can induce a lack of information since they are statistically computed. Hence, high accuracy optical measurements apparatus were developed in the last decades leading to opening new perspectives in surface quality control.

**Fig. 1** FDM process parameter Ishikawa classification (reproduced from Ouazzani et al. [25])

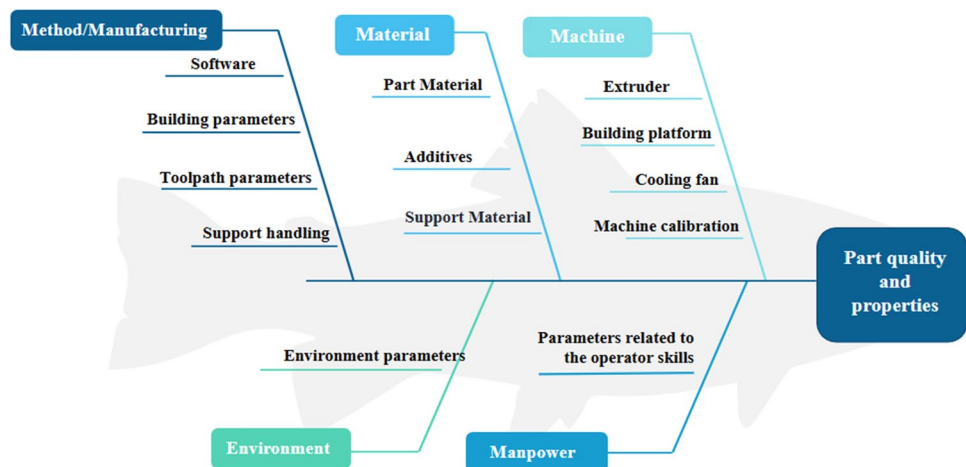


**Table 1** FDM process parameters that impact surface quality

Category	Sub-category	Process parameters
METHOD	Software	Slicing
	Building parameters	Building orientation
	Toolpath/filament parameters	Layer thickness; filament width; filament angle; air gap; contour width
	Post-processing	Support removal method; surface finish processes/treatments; annealing
MACHINE	Extruder/nozzle parameters	Nozzle diameter; extruder speed; extrusion temperature
	Printing bed and cooling parameters	Bed temperature

In the present work, high-precision optical-based equipment is exploited to quantify the input parameters' interplay effect on the surface roughness of the samples. For a wide roughness characterization, this apparatus provides 2D and 3D profiles alike and it allows computing all the corresponding statistics and idealized lines and plans based on least square minimization principle. The rest of the paper is organized as follows; Section 2 exhibits the material and methods adopted in this work; Section 3 displays the results of the investigation, provides the corresponding discussion, and presents the benchmark analysis performed herein. The paper finally is concluded with Section 3.2 that highlights the main results and perspectives of the present work.

## 2 Materials and methods

This section exhibits the materials and methods adopted in this investigation, and it is divided into four main categories:

- A brief presentation of the material to be printed (Section 2.1);
- The design of experiments that produced the process parameter combinations (Section 2.2);
- The FDM, as the processing technology of the samples (Section 2.3);
- The optical samples' surface characterization (Section 2.4);

### 2.1 Materials

As mentioned previously, the material adopted to be processed by FDM technology corresponds to the ABS copolymer. This material is a common thermoplastic polymer that is composed of three monomers, namely, acrylonitrile, butadiene, and styrene. ABS is widely used in a plethora of applications since it shows beneficent compromise gathering toughness, impact resistance, and heat resistance as it is detailed in Tables 2 and 3.

From a material standpoint and regardless of the processing and post-treatment effects, the mechanical properties of the ABS family depend on four main aspects [28–32]:

- Elastomer rate;
- Nodules' dimensions and dispersion in the rubbery phase;
- Reticulation density of the rubbery phase;
- Graft level of the acrylonitrile styrene on the nodules;

In this work, the material is furnished as a bobbin having 1.75 mm of filament diameter (ABS NW- F00200) from TAG3D trademark.

### 2.2 DoE and parameters

In experimental research, one can attest to the unavoidable need to adopt a robust and reliable design of experiments (DOE) before performing any processing, characterization, or analysis. Generally speaking, a DOE is required to minimize the number of Input combinations of an experimental process while ensuring the quality of the generated and computed data. Hence, experts have built experiment plans to be implemented so that the computed models show robustness and reliability regarding the objectives of each engineering area, experimenter, or researcher. For instance, Box-Behnken [48, 49], central composite design (CCD) [35], or Taguchi experiment plans [14, 40, 50] are all widely used techniques in both industry and research according to the expectations and specifications of each project.

In the present research, Taguchi orthogonal arrays (OA) was adopted as a scanning plan so that the FDM processing

**Table 2** Averaged ABS-M30 tensile properties produced by FDM<sup>(1)</sup> according to STM D638 [33]

Mechanical properties	XZ axis <sup>(2,3)</sup>	ZX axis <sup>(2,3)</sup>
Yield strength (MPa)	30.8 (0.85)	27.5 (0.28)
Yield elongation (%)	1.8 (0.043)	1.7 (0.13)
Strength at break (MPa)	28.1 (0.58)	26.8 (0.84)
Elongation at break (%)	8.1 (1.5)	1.8 (0.31)
Modulus (GPa)	2.40 (0.080)	2.30 (0.16)

<sup>(1)</sup>Extract from Table 5 of [33]

<sup>(2)</sup>The values between parentheses are standard deviations

<sup>(3)</sup>The directions of scanning are displayed in Fig. 8 of Appendix 1

**Table 3** Physical properties of ABS family

Thermal properties	
Heat resistance	Authors reported a moderate [34] to relatively good [35] heat resistance of ABS
Use temperature	ABS can be used best within a temperature range of $-20\text{ }^{\circ}\text{C}$ and $80\text{ }^{\circ}\text{C}$ [34]
Glass transition temperature $T_g$	Various values ranging from $100$ to $120\text{ }^{\circ}\text{C}$ were reported. For instance, some works reported $105\text{ }^{\circ}\text{C}$ for some [36] whereas $110\text{ }^{\circ}\text{C}$ for others [37] Other researchers used the DSC method ( <i>differential scanning calorimetry</i> ) to find experimental values of $T_g$ . $102\text{ }^{\circ}\text{C}$ was recorded for Virgin ABS by [34] and $99\text{ }^{\circ}\text{C}$ by [38]. [39] found $114\text{ }^{\circ}\text{C}$ for pure ABS (thermoformed), while $110.44\text{ }^{\circ}\text{C}$ was noted for non-recycled ABS in [40]
Heat capacity $C_p$	The report [41] stated a heat capacity of $1500\text{ J/kg}\cdot\text{K}$ , while [42] reported a value range of $1080\text{--}1400\text{ J/kg}\cdot\text{K}$
Thermal conductivity $\kappa$	A value of $0.18\text{ W/m}\cdot\text{K}$ was reported for pure ABS by Song [43] and $0.17\text{ W/m}\cdot\text{K}$ by [42] Meanwhile, [41] noted a higher value of $0.26\text{ W/(m}\cdot\text{K)}$
Thermal diffusivity $\alpha$	A value of $1.65 \times 10^{-7}\text{ m}^2/\text{s}$ — at room temperature — was reported by [41]
Thermal shrinkage	ABS is known for its dimensional stability [44] with relatively acceptable thermal shrinkage [45]. Some suppliers reported a range of $0.7\text{--}1.6\%$
Optical properties	
Glossiness	ABS is known for its glossy appearance, with “styrene” being the responsible element for that “glossiness” [35]. Some ABS suppliers reported glossiness rates ranging from $40$ to $96\%$
Opacity	ABS is naturally opaque or translucent white, depending on particle size distribution [46]. Pigments can be added to obtain different colors
Sensibility to UV rays	Pure ABS is notorious for its poor resistance to UV radiation. It undergoes discoloration and damage under direct sunlight. Amendola et al. was one of the earliest researches that observed the discoloration and absorbance increase of ABS under thermal treatment [47]

parameters were got at a first glance as equivalent in terms of complexity; that is to say, no additional constraints were considered in terms of parameters tuning or varying. Indeed, it was proven in a rich literature that Taguchi OA provided statistically reliable results, while the number of experiments is well reduced which lead to a significant time and material saving [51].

Five different factors and with three levels each were selected herein in order to understand the quality surface evolution regarding the FDM processing as it is exhibited in Table 4. In addition, Table 5 exhibits the factors combinations selected according to Taguchi L27 OA.

The input factors (controlled parameters) are presented in the following list.

- Processing parameters that are:
  - o The layer thickness;
  - p The extrusion nozzle temperature;
  - q The printing speed;

**Table 4** List of parameters adopted in the present study and the corresponding levels

Parameters	Unit	Notation	Level 1	Level 2	Level 3
Layer thickness	mm	Lth	0.1	0.2	0.3
Extrusion temperature	$^{\circ}\text{C}$	Temp	240	250	260
Printing speed	mm/min	Spd	2000	3000	4000
Heat treatment*		H.T	HT1	HT2	HT3
Tensile speed*		Tens. Spd	D1	D2	D3

- Post-treatment parameter: heat-treatment temperature;
- Tensile test strain-rate;

Note that it is worth mentioning that the present study is not dedicated to the mechanical properties analysis of the manufactured samples, even though the tensile test strain rate was listed as a parameter. Actually, this latter will be exploited in a future study, but it was also included in the experiments plan so that the number of samples to be tested was multiplied by three, which corresponds in fact to the level of repetitiveness required for a reliable statistical analysis of the produced data. Indeed, this is what advised by the standards such as the ASTM S368-14 and other experimentation standards.

Hereafter, a multiway ANOVA analysis was carried out in order to highlight the most significant factors that are involved in the roughness variability of the samples; a threshold of  $5\%$  regarding  $p$ -value was selected as it is classically adopted in the literature. After all, response surfaces (RS) are exhibited in the study; the factors' effects and interactions charts were plotted in order to visually appreciate the numerical results pointed-out by means of the multiway ANOVA analysis. All data analytics were handled and programmed by means of Matlab 2022 platform.

### 2.3 FDM printer and the tested specimens

In this study, the tensile specimens ASTM D638 Type IV were adopted since they were produced also for the future tensile tests. Figure 2 a exhibits the corresponding shape and

**Table 5** L27 Taguchi-based orthogonal array

Sample no	Lth	Temp	Spd	Tens. spd	H.T
1	1	1	1	1	1
2	1	1	2	1	1
3	1	1	3	1	1
4	1	2	1	2	2
5	1	2	2	2	2
6	1	2	3	2	2
7	1	3	1	3	3
8	1	3	2	3	3
9	1	3	3	3	3
10	2	1	1	3	2
11	2	1	2	3	2
12	2	1	3	3	2
13	2	2	1	1	3
14	2	2	2	1	3
15	2	2	3	1	3
16	2	3	1	2	1
17	2	3	2	2	1
18	2	3	3	2	1
19	3	1	1	2	3
20	3	1	2	2	3
21	3	1	3	2	3
22	3	2	1	3	1
23	3	2	2	3	1
24	3	2	3	3	1
25	3	3	1	1	2
26	3	3	2	1	2
27	3	3	3	1	2

dimensions and presents the areas involved in the roughness optical measurement; the red line as for the 2D roughness profiles while the blue area expresses the surface area involved in 3D surface profiles plot.

As for the FDM printing machine, VOLUMIC Stream 30 Ultra was adopted; it is available in the Euromed Center of research of Euromed University of Fes, Morocco. All specimens were positioned at the center of the building plate in order to ensure the same processing environmental conditions and to avoid thermal deviation that should be denoted between the tested specimens. The VOLUMIC Stream 30 characteristics are displayed in Table 6. In addition, samples were produced at a 100% filling with a continuous scanning of  $-45^\circ/45^\circ$  path as displayed in Fig. 2b. The orientation of the samples during printing corresponds to the XY orientation with regards to Fig. 8 of Appendix 1.

**Remark** The frame of reference displayed in Fig. 2 a and b is indirect since it is the same as for the frame of reference adopted in the 3D profiles figures provided by the optical roughness measurement apparatus.

## 2.4 Surface quality characterization

### 2.4.1 Roughness measurement instrument (Altisurf 500)

Apart from the classical Stylus-based measurement tools, optical apparatus have been developed based on various optical physics and the associated techniques. These methodologies usually obtain the part's surface topography using an incident light source. Due to their accuracy, they are more dependable and statically relevant than the classical stylus-based measurements.

In this study, “Altisurf” roughness measurement apparatus, presented in Fig. 3, was utilized (Fig. 3) alongside the software “AltiMap” (AltiMap Standard 6.2.6746) to obtain 3D scanned images of the surfaces additionally to the 2D roughness profiles. This apparatus is provided by the Mechanic, Mechatronic and Command Laboratory, ENSAM, Moulay Ismail University, Meknès, Morocco. In addition, Table 7 summarizes the essential of Altisurf 500 features.

### 2.4.2 Standards

The standard adopted for the profiling parameters is the ISO 4287 (revised by ISO 21920–2:2021). It defines the primary, waviness, and roughness (2D) profiles as well as the associated geometrical parameters. A cut-off value of “ $\lambda_c=0.8$  mm” with a “Gaussian filter” was adopted as recommended in the standards text that are adopted by the apparatus.

According to the standards, the three profiles listed in the previous paragraph are linked by Eq. 1, according to which the “waviness” and the “roughness” profiles are respectively filtered low-pass and high-pass. In addition, the waviness profile is usually related to the manufacturing process and the associated instabilities, while the roughness profile reflects the actual surface microstructure. That is why particular attention was assigned to the roughness profiles and to the related parameters.

$$\text{Primary profile} = \text{Waviness profile} + \text{Roughness profile} \quad (1)$$

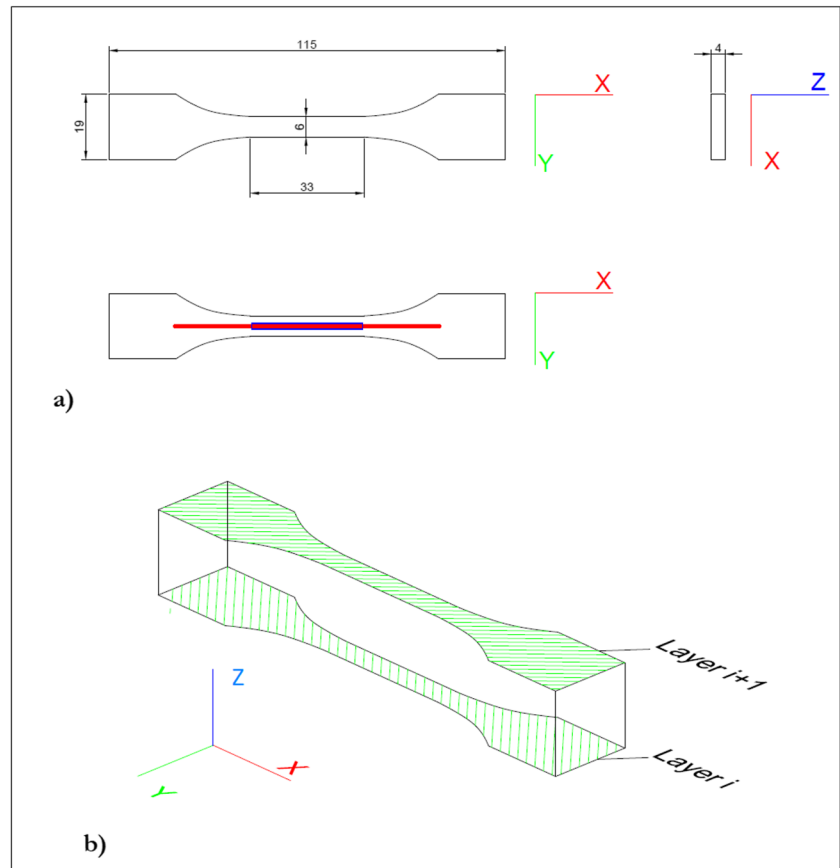
The measurement apparatus computes the following roughness indicators [ISO 4287]:

- Ra: the arithmetic mean roughness;
- Rq: the root-mean-square deviation;
- Rz: the maximum height of profile;
- Rp: the maximum profile peak height;
- RSm: the mean width of profile elements.

For more details regarding roughness indicators, the reader is referred to references such as [52, 53]. As for Surface (3D) images and parameters, the ISO 25178 standard was adopted as it is prefixed by the apparatus.



**Fig. 2** **a** Tensile specimen's dimensions with red line for the 2D roughness profiles; blue area for 3D surface profiles. **b** Scan filling pattern as  $-45^{\circ}/45^{\circ}$  orientations.



### 3 Results and discussion

This section provides the results of the roughness profiles and the corresponding multiway ANOVA in order to point-out the most significant factors involved in the roughness analysis.

**Table 6** Volumic stream 30 printer specifications

Features	Range/value
FDM printer model	VOLUMIC Stream 30 Ultra
Maximum printing volume ( $\text{mm}^3$ )	290(X) $\times$ 200(Y) $\times$ 300(Z)
Number of nozzles	1
Nozzle diameter (mm)	0.4
Maximum nozzle temperature ( $^{\circ}\text{C}$ )	420
Maximum bed temperature ( $^{\circ}\text{C}$ )	150
Maximum printing speed (mm/s)	300
Positioning precision (Z)	1 $\mu\text{m}$
Positioning precision (X–Y)	15 $\mu\text{m}$
Slicing software	Simplify 3D
Building direction	Z axis

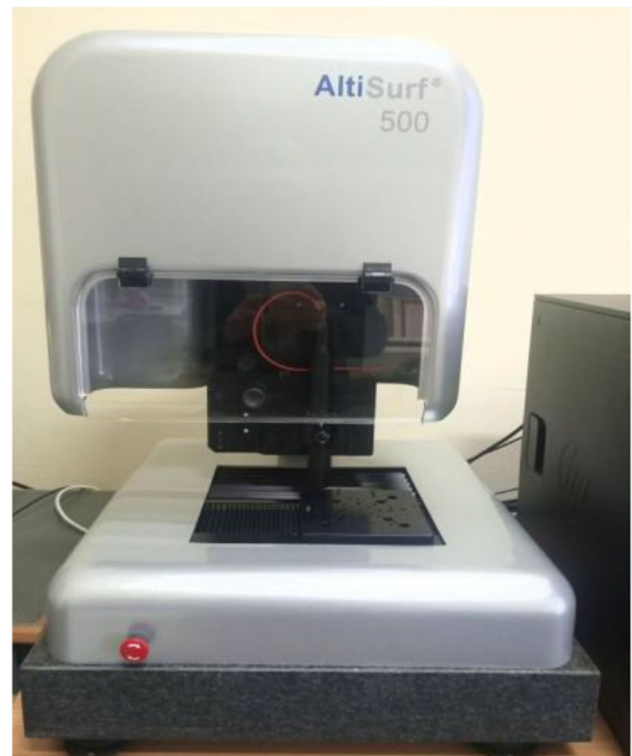


**Fig. 3** Altisurf 500 roughness measurement apparatus

**Table 7** Optical metrology instrument specifications (Altisurf 500)

Features	Range/value
Measuring instrument	Altisurf © 500
Sensor type	Non-contact (chromatic confocal)
Analysis software	Altimet ®
Dimensions (mm)	100(X)×100 (Y)×100(Z)
Maximal speed (mm/s)	40

### 3.1 Roughness topography and the related statistics

Figure 4 a and b depict the 2D and 3D profiles of respectively sample nos. 7 and 26 as illustrative profiles’ samples that were measured by means of the optical measurement apparatus “Altisurf 500.” The measurement direction corresponds to the Z axis as it is displayed in Fig. 4b.

The 2D profile reports the roughness as the actual positive and negative distances that are computed according to the geometric center-plane defined as the null plane, while the 3D profile displays in a map color the positive distances according which the null value correspond to the lowest z level cavity. The rest of the figures are exhibited in Appendix 7. with regard to the samples’ numbering.

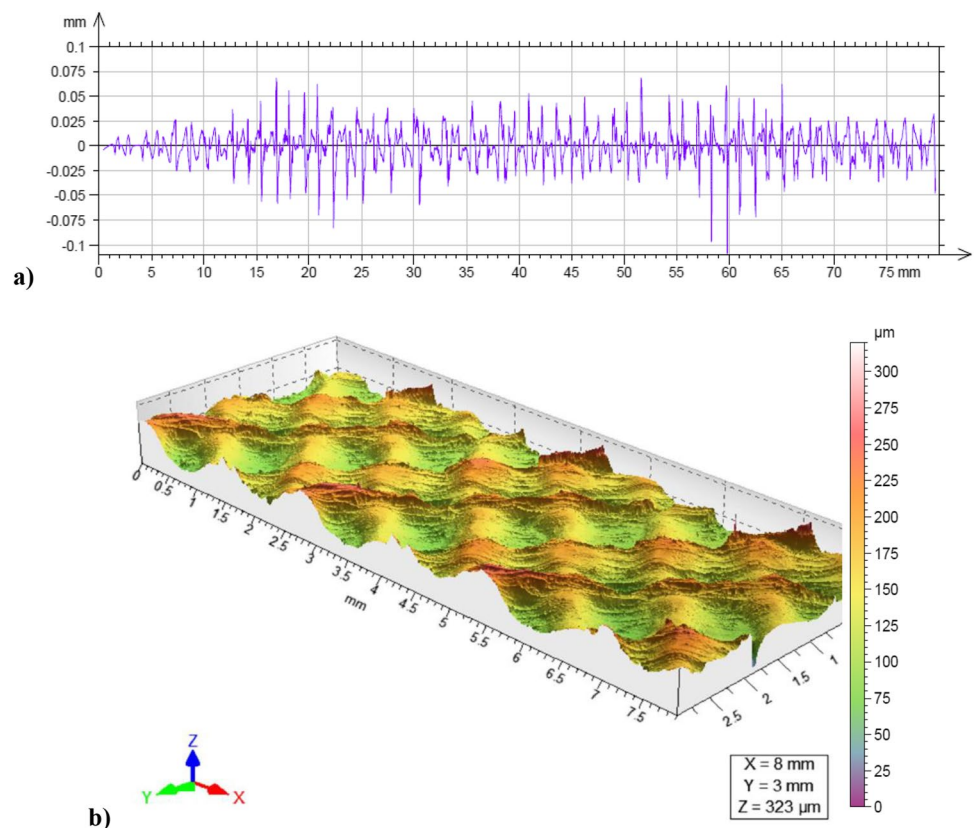
On the 3D profiles, one can observe the 45°/–45° printing directions but also the empty spaces or low Z coordinates that correspond to the surface matter density which does not reach the maximum, even if the infill was set to 100% in the printing parametrization. This can be due to the ovalness of the filaments which are supposedly not in contact at the surface but which are very near from each other in the middle thickness of the filaments. These spaces can also the result of filaments’ shrinkage which, actually, is an inherent phenomenon of this kind of materials and processes.

Table 8 displays the computed roughness indicators of the different samples directly extracted from the software of the measurement apparatus.

### 3.2 Factorial analysis and multiway ANOVA

A multiway ANOVA was carried-out in order to select the most significant processing parameters that are involved regarding the roughness evolution in the printed sample surfaces. In addition, response surfaces, effects, and interactions charts were plotted in order to visually point-out the evolutions computed by means of the ANOVA analysis. In consequence, in this section, the detailed results with regard to the arithmetic roughness Ra are displayed as:

**Fig. 4** Scanned profile: a 2D profile of sample no. 7; b 3D profile of sample n. 26



- Fig. 5 shows the multiway ANOVA table and SR according to the different inputs;
- Fig. 6 exhibits the multivariate chart of the simple effects graphics;
- Fig. 7 displays the pairwise interaction charts regarding all the input variables;

while the related graphics of Rq, Rz, Rp, and RSm roughness indicators are displayed in detail in Appendix 8. that groups both ANOVA tables and the response surfaces. Furthermore, Appendix 9. is dedicated to the DoE factors' effects and interactions plots.

The multivariate charts displayed in Fig. 6 and in Figs. 14, 15, 16, 17, and 18 of Appendix 4 allow compacting the simple factor effect visualization in a unique chart. For instance, in order to understand the temperature's effects in these figures, it is mandatory to hold a given scan speed; after that, a value of Lth should be also held, and finally, the effect of the temperature change is to be locally read by following the links between the little dots that are presented as a set of {circle,

diamond, square} for each value of the extrusion temperature. In addition, as classically known concerning the DEO charts' interpretation, sharper is the slope between the dots, highest is the effect with regards to the corresponding levels' values.

Hence, by projecting the latter rules on Figs. 6, 14, 15, 16, 17, and 18, one should note the insignificant of the temperature parameter variation as a simple effect on all the roughness indicators; in other words, no reasonable variation can emerge from temperature change. In a same way, the scan speed parameter Spd has not shown a salient effect on the behavior of the response, or in other terms, a random behavior was denoted concerning the simple Spd's effects.

On the other side, the interactions' charts showed interesting outcomes as an apparent behavior change in the response according to:

- the interactions “Lth \* Temp” and “Lth \* Spd” in the case of Ra (Figs. (7) or 14), Rq (Fig. 15) roughness indicators;
- the interactions “Lth \* Temp” as for RSm (Fig. 18);

Contrariwise, low intense interactions' effects were denoted for Rp indicator, and unlike Rz output which showed very random and really insignificant graphical behavior. Nevertheless, the above discussion must be enriched by means of the multiway ANOVA which remains the ultimate quantitative tool for interpreting such findings.

### 3.3 Discussion and benchmark analysis

To sum up, the most significant factors are reported in Table 9 with the corresponding outputs and *p*-values; Table 9 statistics were selected from the ANOVA tables of Figs. 9, 10, 11, 12, and 13 of Appendix 3.

According to Table 9, one should note that the layer thickness Lth should be considered as the most significant factor of this investigation since it is clearly involved in the majority of the roughness indicators (output) with a low *p*-values that are less than 5%. Indeed, Lth is involved in the case of Ra, Rq, and RSm as a simple effect factor; while it was significantly involved in the Rp indicator as a simple effect factor with a *p*-value of 0.12%, and in the interactions in the way that it is combined to the extrusion temperature (Temp) at *p*-value of 4.40%. In addition, the scan speed (Spd) is involved as a simple factor at *p*-value of 2.57%, and in the interaction with the extrusion temperature at *p*-value 3.09%. Hence, it is noticeable with regard to the *p*-values that the simple effect of Lth takes place with a higher precision than the interactions, which, in fact, still remain valid alike.

In the other hand, concerning the Rz indicator, one should remark that no significant factor emerged from the ANOVA; it can be the case since the Rz is the average value of the absolute values of the heights of “five” highest-profile peaks

**Table 8** Roughness statistics of the top face according to the Z axis

Try no	$R_a$ ( $\mu\text{m}$ )	Rq ( $\mu\text{m}$ )	Rz ( $\mu\text{m}$ )	Rp ( $\mu\text{m}$ )	RSm (mm)
1	8.39	11.1	45.4	20.5	0.581
2	10.5	15.1	62.5	23.8	0.522
3	7.18	9.18	36.5	17.6	0.643
4	9.04	12.1	49.9	22.5	0.546
5	8.34	10.3	40.3	20.1	0.566
6	10.2	13.8	57.4	26.2	0.538
7	8.97	11.9	49.9	23.4	0.560
8	9.63	12.7	52.7	23.8	0.581
9	7.32	9.67	39.4	18.5	0.522
10	11.7	14.5	54.5	31.0	0.602
11	11.3	14.1	53.9	27.5	0.543
12	11.7	14.3	54.2	25.0	0.576
13	9.12	11.6	44.5	22.8	0.543
14	11.1	13.7	50.7	23.6	0.560
15	8.87	11.8	46.3	24.0	0.689
16	11.0	14.3	56.6	29.9	0.554
17	11.7	15.7	64.3	33.5	0.550
18	9.55	12.4	48.4	24.1	0.640
19	12.0	15.4	57.6	27.7	0.730
20	11.6	15.4	59.6	27.2	0.520
21	12.0	14.8	53.7	25.6	0.643
22	11.5	14.4	54.2	26.3	0.663
23	12.3	16.5	66.2	29.9	0.672
24	13.4	16.4	60.5	27.9	0.682
25	12.5	15.6	58.7	27.9	0.775
26	10.5	13.9	54.8	28.3	0.610
27	9.03	11.3	41.4	20.1	0.758



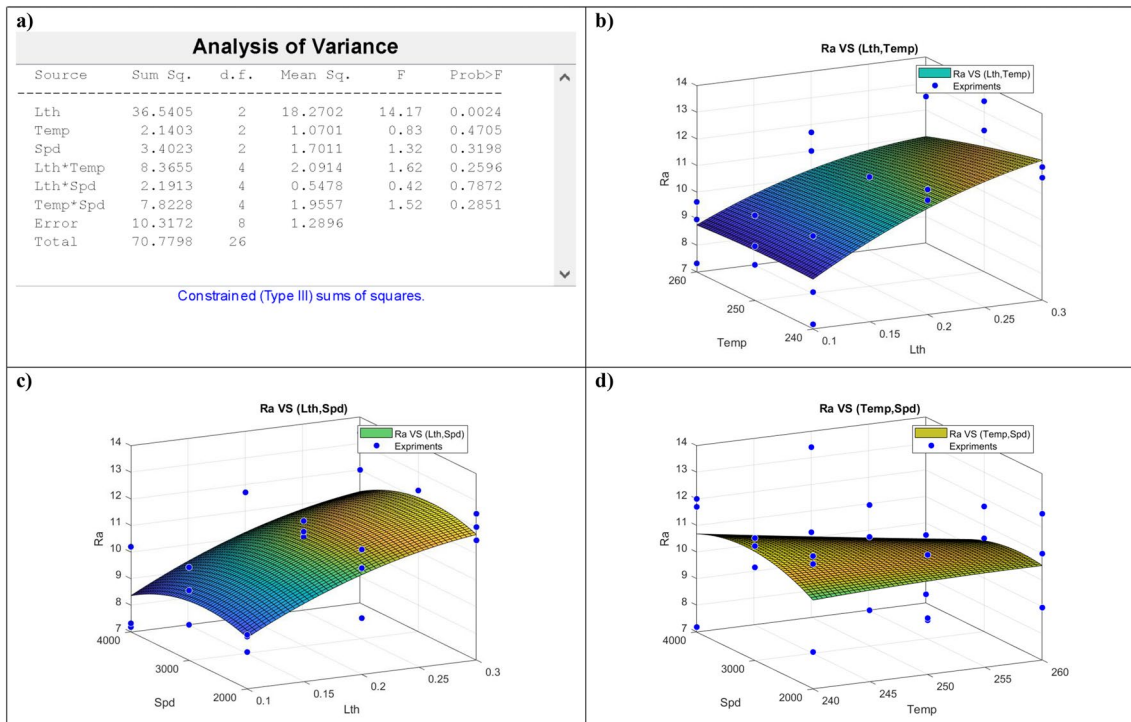


**Fig. 5** Ra roughness ANOVA and the corresponding response surface: a ANOVA table. b RS of Ra VS {Lth, Temp}. c RS of Ra VS {Lth, Spd}. d RS of Ra VS {Spd, Temp}

**Fig. 6** Multivariate chart of the simple effects graphics regarding Ra roughness according to {Lth, Temp, Spd} parameters

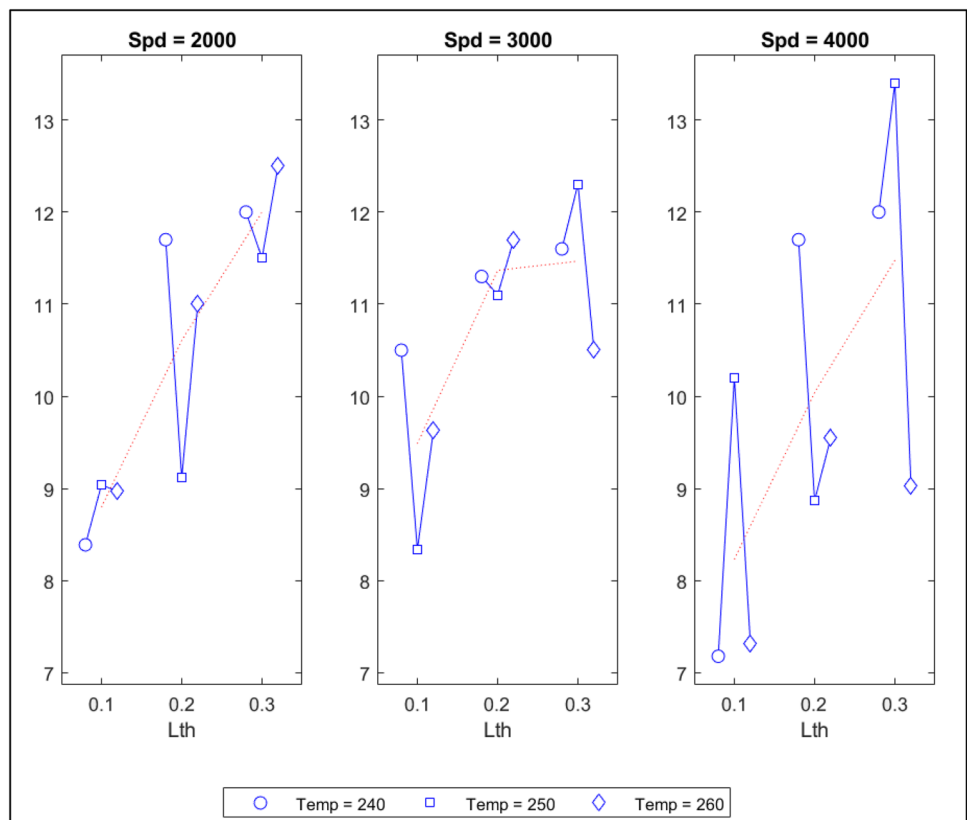
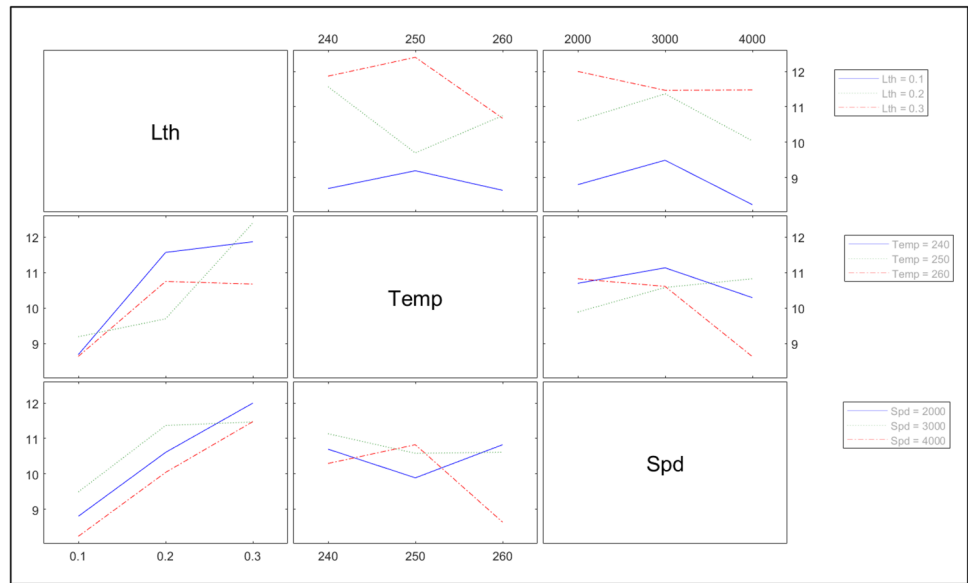


**Fig. 7** Interactions' chart of Ra roughness according to {Lth, Temp, Spd} parameters



and the depths of “five” deepest alleys within the evaluation length. That is to say, only 10 values are included in the calculation of Rz indicator, which is in fact very weak from a statistical standpoint. In consequence, the authors think that it is quite reasonable to obtain such insignificant relationships between Rz and the processing parameters.

Moreover, a benchmark analysis was carried-out in order to position the present work within the literature map. Hence, Table 10 includes number of existing works that characterized the upward surfaces as it was treated in this paper.

Other works such as Jiang et al. used PLA material and have found that the roughness values differed depending on the measurement direction. Ra was estimated around 32  $\mu\text{m}$  along the building direction, while it is ranged around 5  $\mu\text{m}$  for the scan directions (across filaments) [23]; similar analysis showed Ra between 15.38 and 22.84  $\mu\text{m}$  [57].

Unlike the high interest in Ra, only a few works were interested in other parameters, such as the mean peak width RSm and maximum profile peak height Rp. As for Hall et al. [58], RSm values ranged from 0.156 to 0.400 mm, while the

manufacturing targeted RSm at 0.2 mm; the authors denoted the difference for various materials processed by FDM. On the other hand, an average value of 0.486 mm was noted for FDM parts in [16]. As for our specimens, RSm falls within a range of 0.520 to 0.775 mm, although the “filament width” parameter was constant to a value of 0.4 mm (equal to Nozzle diameter). This difference is mainly due to the shape of filaments after deposition shows a likely oval shape leading to increase the width of filaments.

Based on the above, the following points highlight the most important factors that are involved in the surface finish:

### 3.3.1 Scan speed

According to the present literature survey, various works such as [23, 59], and [27] stated that “printing/deposition speed” affects the FDM parts’ surface. Chohan et al. [56] also suggested that low printing speed may result in a better surface finish.

However, experimental works such as [17] noticed a non-linear behavior of roughness based on the corresponding S/N ratio calculation. Same for the present work, minimal values of roughness were denoted at 4000 mm/min, while maximal values were caught for 3000 mm/min. Thus, the best surface was achieved at the highest level of speed 4000 mm/min. This was shown more clearly in Appendix 7, from 3D images of samples 13–15, and 2D images of samples 1–3 and 16–18, as the maximal speed surfaces (last) were of the best quality.

This variation can be explained by the fact that high speed affects the material viscosity; as filament cooling is delayed, the bonding between adjacent filaments is better, and this led to better surface quality and to a decrease in the apparent dimension of the filament, and hence a decrease of the roughness.

**Table 9** The most significant factors and outputs

Output	Factor/interaction	p-value (%)
Ra	Lth	0.24
Rq	Lth	1.43
Rz	—	—
Rp	Lth	0.12
	Spd	2.57
	Lth * Temp	4.0
	Temp * Spd	3.09
RSm	Lth	0.35

**Table 10** Roughness results from literature

Works	Printing –Input-parameters	Results
Kattethota and Henderson 1998 [54]	- Layer thickness - Orientation angle	Ra varied depending on inclination angle: - from 12.7 to 58.42 $\mu\text{m}$ for Lth of 0.254 mm (0.010") - from 12.7 to 35.56 $\mu\text{m}$ for Lth 0.178 mm (0.007") Concerning the 90° inclination angle, Ra was around 12.7 $\mu\text{m}$ for both Thickness levels
Anitha et al. 2001 [17]	- Speed deposition - Layer thickness - Road width	Ra values ranged between 2.63 and 10.73 $\mu\text{m}$ ;
Badola and Vaishya 2016 [55]	- Contour Width - Build style	Roughness ranged between 10.76 and 14.30 $\mu\text{m}$ with a variant contour width;
Chohan and Singh 2017 [27]	Smoothing cycles (reduction of the roughness)	Initial values of Ra (before surface smoothing) were around 9 $\mu\text{m}$ ;
Rajesh et al. 2021 [50]	- Layer height - Temperature	Ra: values were between 23.25 and 31.92 $\mu\text{m}$ ;
Chohan et al. 2022 [56]	- Nozzle temperature - Printing speed - Infill pattern	Ra values ranged between 1.50 and 2.64 $\mu\text{m}$ ;
Xu et al. 2000 [16]	Different AM processes (FDM, SL, SLS, LOM)	Ra = 18.28 $\mu\text{m}$ for the FDM process;
The present work	- Printing speed - Layer thickness - Extrusion temperature	Variation of roughness as a function of different parameters: - Printing speed: in simple effects and interaction - Layer thickness: in simple effects and interaction - Extrusion temperature: as an interaction effect

### 3.3.2 Layer thickness

Based on literature review, surface roughness decreases for lower “layer thickness/height” [17, 50, 54, 57]. After reviewing various works, Chohan and Singh (2017) also reported that many of them reached the best surface finish for minimal thicknesses [27]. Haque et al. obtained similar results using Ra numerical calculations values so that it increased for higher layer thickness [60].

The present findings show similar roughness behavior with literature. The authors also denoted the smoothest surface quality for the lowest layer thickness which was set at 0.1 mm before printing. Meanwhile, the highest variations were noticed for higher thickness levels. A small difference in the last set, where specimen no. 17 showed abnormal peaks, as exhibited in the specimen’s 2D profile (Appendix 7.), this can be due to residue of anti-warping glue utilized in the printing process.

This tendency can be understood regarding the stair-stepping phenomenon which appears at higher layer thickness in the FDM process. Hence, decreasing the thickness should imply the decrease of the stair-stepping effects in FDM parts which should generate better surface finish; layer thickness has also an effect on filaments bonding, and then on the final surface.

### 3.3.3 Extrusion temperature

According to literature works, “3.3.3” plays a crucial role in FDM surface quality [27, 50, 56]. Results of their

experiments showed that smoother surface finish can be attained using low nozzle temperature.

According to the present findings, it is noticeable that the temperature of 250 °C was in general optimal for surface quality. However, specimens 8 and 25 were subject to apparent warping during printing which should explain the unexpected some high values of roughness even at high temperature. This was also observed in 3D profiles representation of Appendix 7., as they depict best surface quality at highest temperatures. This can be remarked from the observation of 3D profiles in Appendix 7. of specimens {1, 4, 7} (1st set), {2, 5, 8} (2nd set), and {19, 22, 25} (3rd set).

Indeed, temperature directly affects the part’s roughness. As the temperature rises, the material ABS does not melt, given it is an amorphous polymer. However, its fluidity changes which affects the surface quality. Moreover, increasing extrusion temperature leads to a rise in cooling time and delay filament solidification. That leads to better bonding between filaments, hence a smoother surface.

## 4 Conclusive remarks and work’s perspectives

The present work aims to identify the most influencing FDM’s processing factors involved in ABS printing samples with regard to the surface quality in terms of different roughness’ indicators. The input parameters selected correspond to the

layer thickness, the extrusion temperature, and the scan speed, while the roughness indicators adopted are the Ra, Rq, Rq, Rz, and RSm which are considered as the output factors of the present investigation. According to the number of factors and levels, L27 Taguchi OA was built in order to statistically study the effects and interactions in a robust and reliable way.

Each sample's surface was scanned with optical Altisurf apparatus, allowing full catching of 3D and 2D profiles of the surfaces' peaks and depths; then, the corresponding roughness indicators were computed by means of the AltiMap software that is provided with the measurement apparatus. After that, a series of statistical analysis were carried-out by means of multiway ANOVA that was applied in order to select the most significant input factors that are involved in the roughness variation. Parallel to that, response surfaces, the simple effects multivariate charts, and the interactions charts were displayed to visually appreciate the evolution of the outputs according to the input factors.

A first conclusive remark concerns the insignificance of the analysis of Rz roughness index which required at most 10 values of the surfaces profile, 5 peaks and 5 depths. This low number constitutes, in fact, an insufficient count of data to be modelled or analyzed using the statistical techniques such as ANOVA analysis or regressive models. Figure 16 of Appendix 4 shows clearly the random behavior of both simple effects and the interactions regarding Rz, which allow attesting that the change in the input levels is not the responsible of Rz variability.

On the other hand, as for the other remaining roughness indicators, the following list highlights the most significant concluding remarks which are based essentially on the quantitative discussion provided by the related ANOVA tables and indices. Hence, these remarks are organized separately with regard to each input factor as follows:

- The layer thickness is involved as a first order factor for Ra, Rq, Rp, and RSm; Lth is also coupled to the extrusion temperature in the interaction term  $Lth * Temp$  regarding Rp index. Furthermore, according to the RS, effects, and interactions charts, it was highlighted that better surface quality, or in other terms low roughness indicators, is linked to low layer thickness that is predefined in the slicing step of the FDM pre-process.
- The extrusion temperature is present in the interactions' terms of the Rp indicator. Indeed, the extrusion temperature was remarked to be linked to both layer thickness and scan speed, and it was not involved as a first order factor. It was also remarked that the middle temperature of 250 °C resulted in better surface quality compared to 240 °C and 260 °C as it is salient from the interactions charts of Appendix 9.. Furthermore, the temperature should affect the rheology of the printed material according to the interactions with the layer thickness, so that a low layer thickness enforced by a low nozzle height locally compresses the matter; it leads to the minimization of the roughness profiles. Nevertheless, this interac-

tion shows very complex behavior such that low temperature can promote stable matter deformation with a minimization of the corresponding shrinkage, but high temperature should facilitate the matter flow horizontally but can flow also onto the neighbor matter resulting in higher roughness.

- On the other hand, the scan speed is also involved only in the roughness Rp; it is present as a simple effect factors but also in the interaction  $Temp * Spd$ . This relationship is significant since the scan speed should affect the appearing diameter of the filament deposit and higher temperature should facilitate the matter flow and reduce the diameter with higher scan speed, and so on. It was denoted finally that lower is the scan speed, higher is the surface quality since the cooling time is delayed, which enhances the bonding between the adjacent filaments and decrease the materials roughness.

To sum up, the roughness behavior shows a complex relationship with the input parameters. Experimentations and statistical analysis can provide cause/effect relationships between the roughness and the processing parameters. Nevertheless, apart to the empirical approach, one should note that a full understanding of this relationship must include phenomenological studies that involve fluid dynamics and rheology, thermal analysis and calorimetry, and advanced physics such as coupling surface tension phenomenon to the previous fluid and thermodynamics. Hence, future works will develop a semi-empirical method based on fluid dynamics and thermodynamics with adopting stochastic parameters for which the variability will be identified according to the experiments. The approach is currently under development for a further implementation with computational fluid dynamics (CFD).

## Appendix 1. Printing directions according to [33]

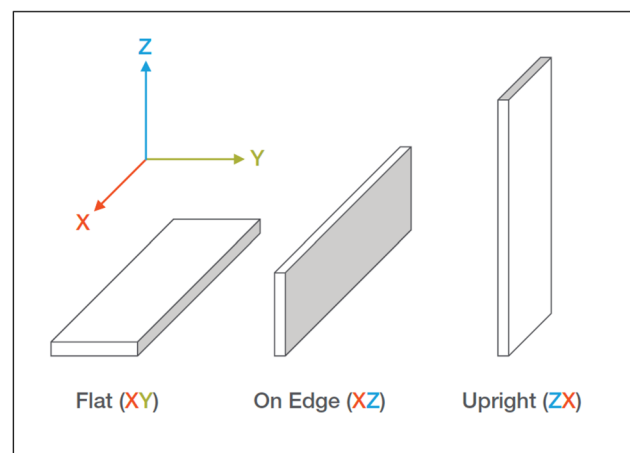
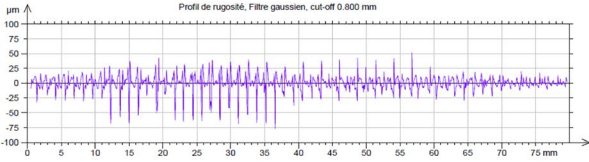
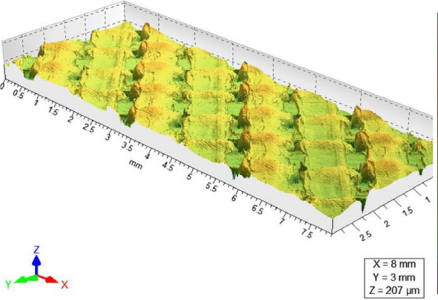
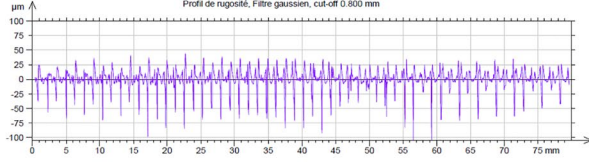
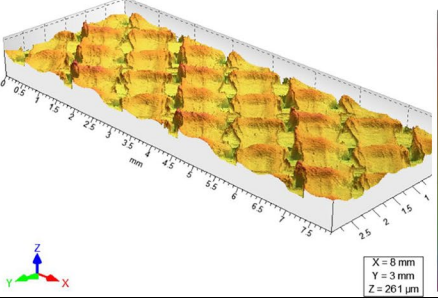
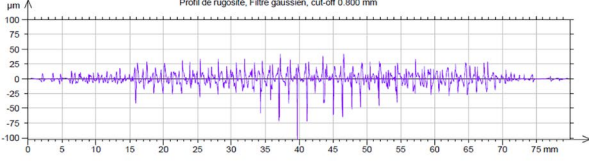
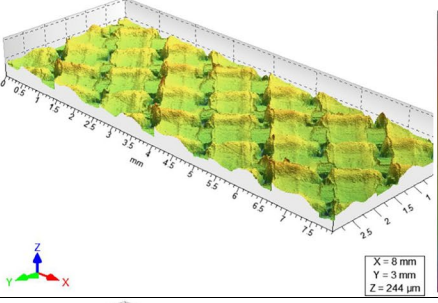
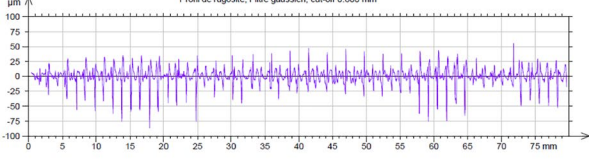
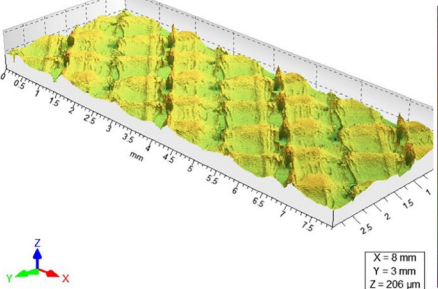
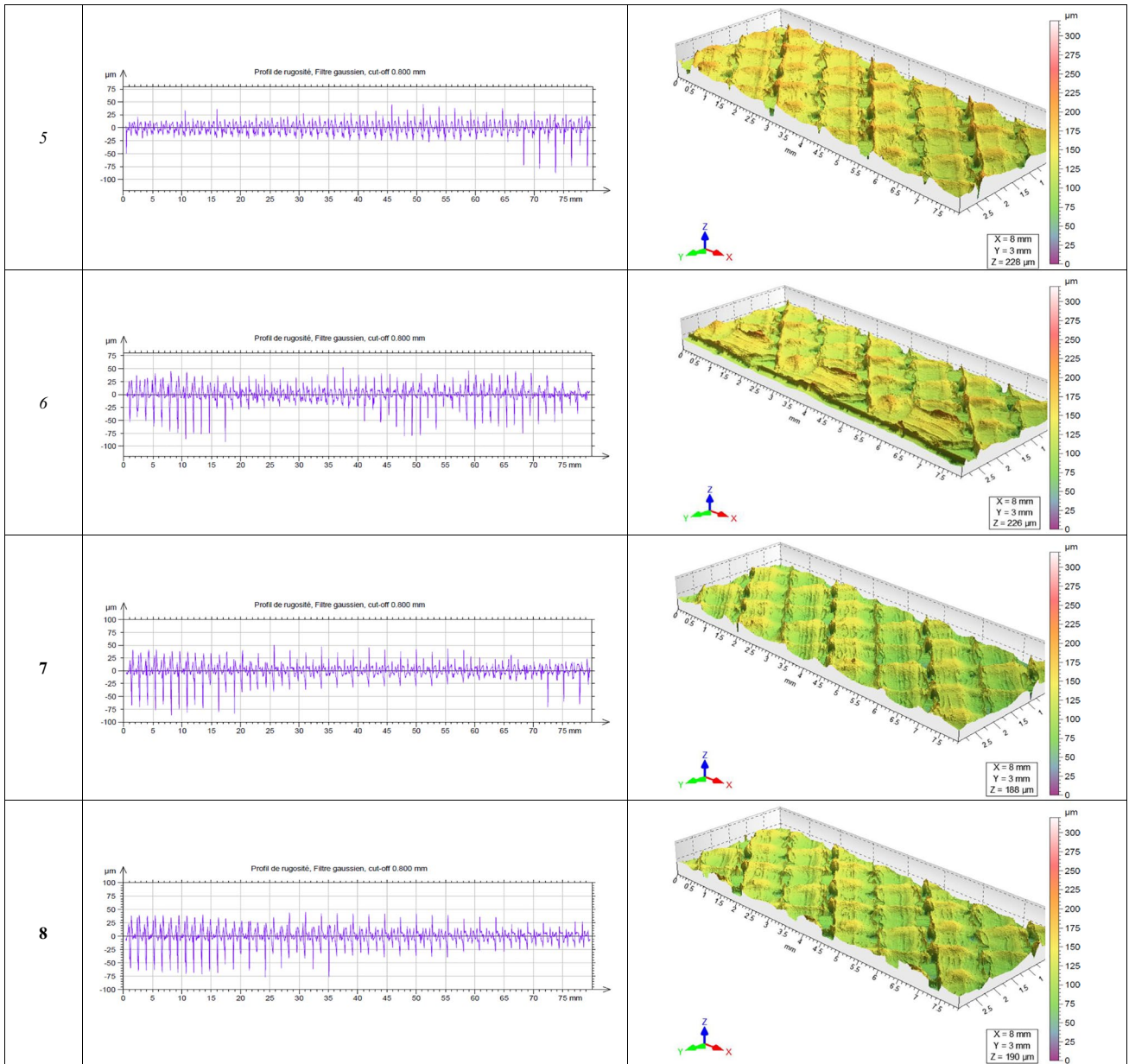


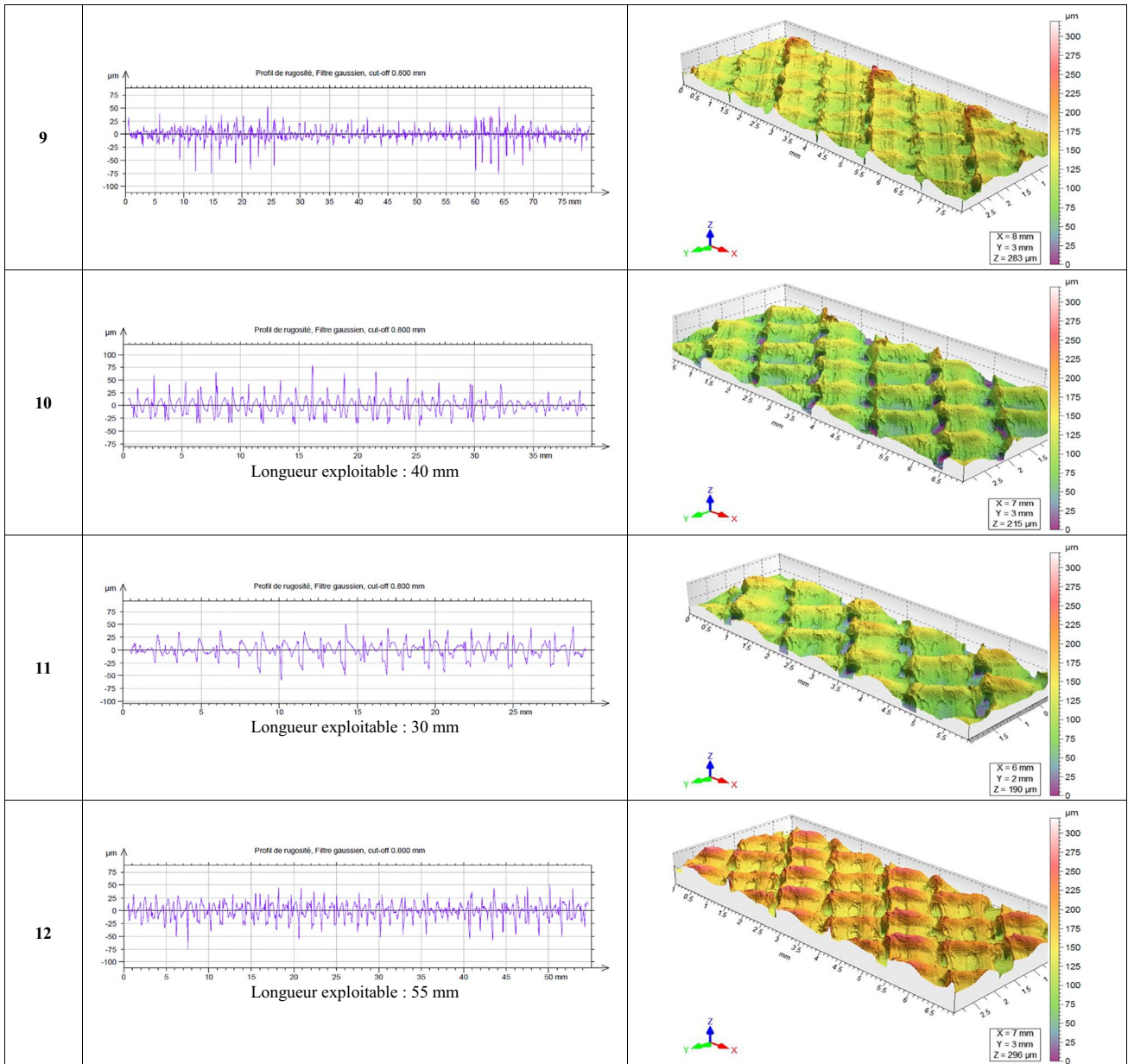
Fig. 8 Scanning directions according to [33]

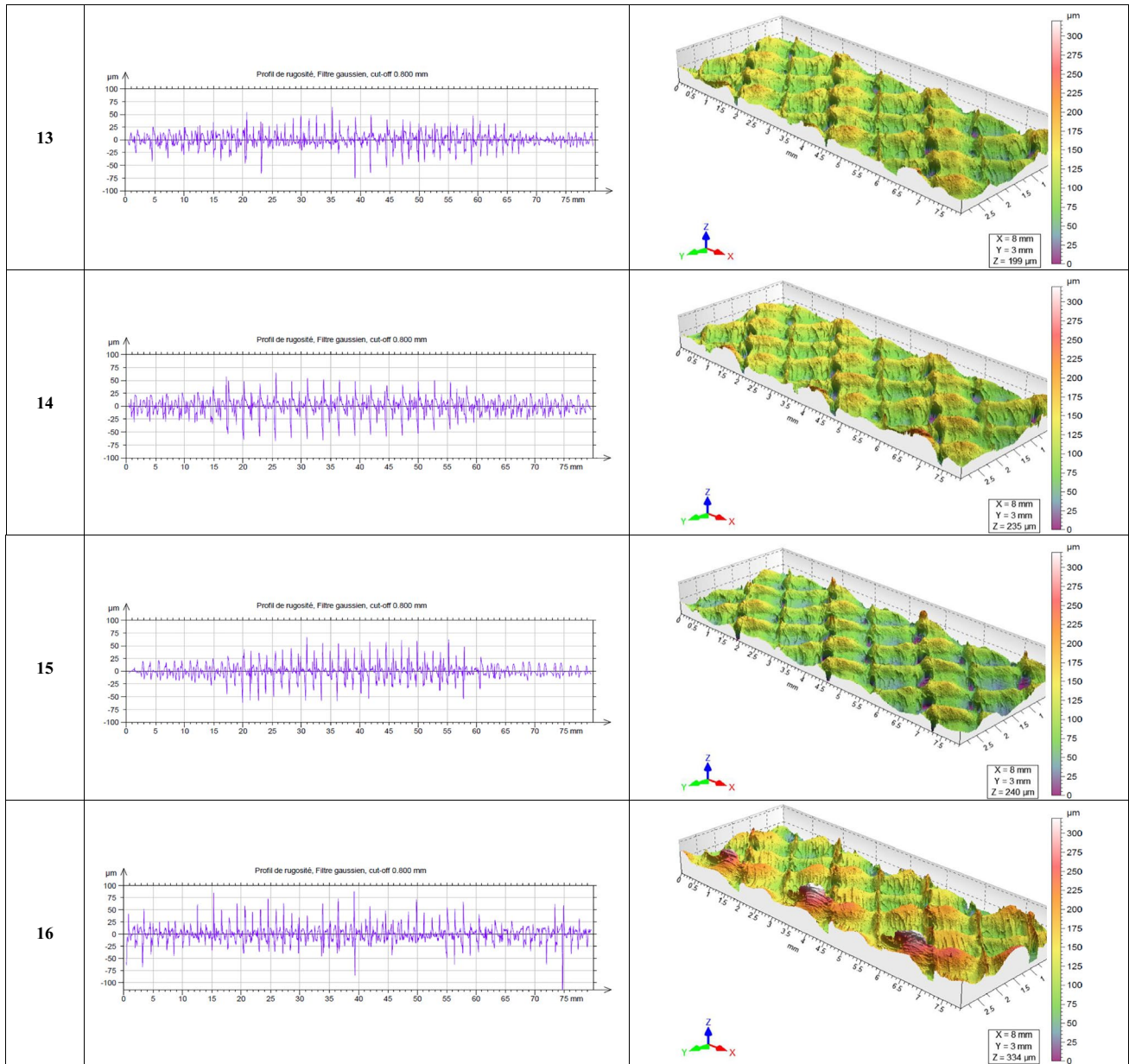
### Appendix 2. 2D and 3D profiles

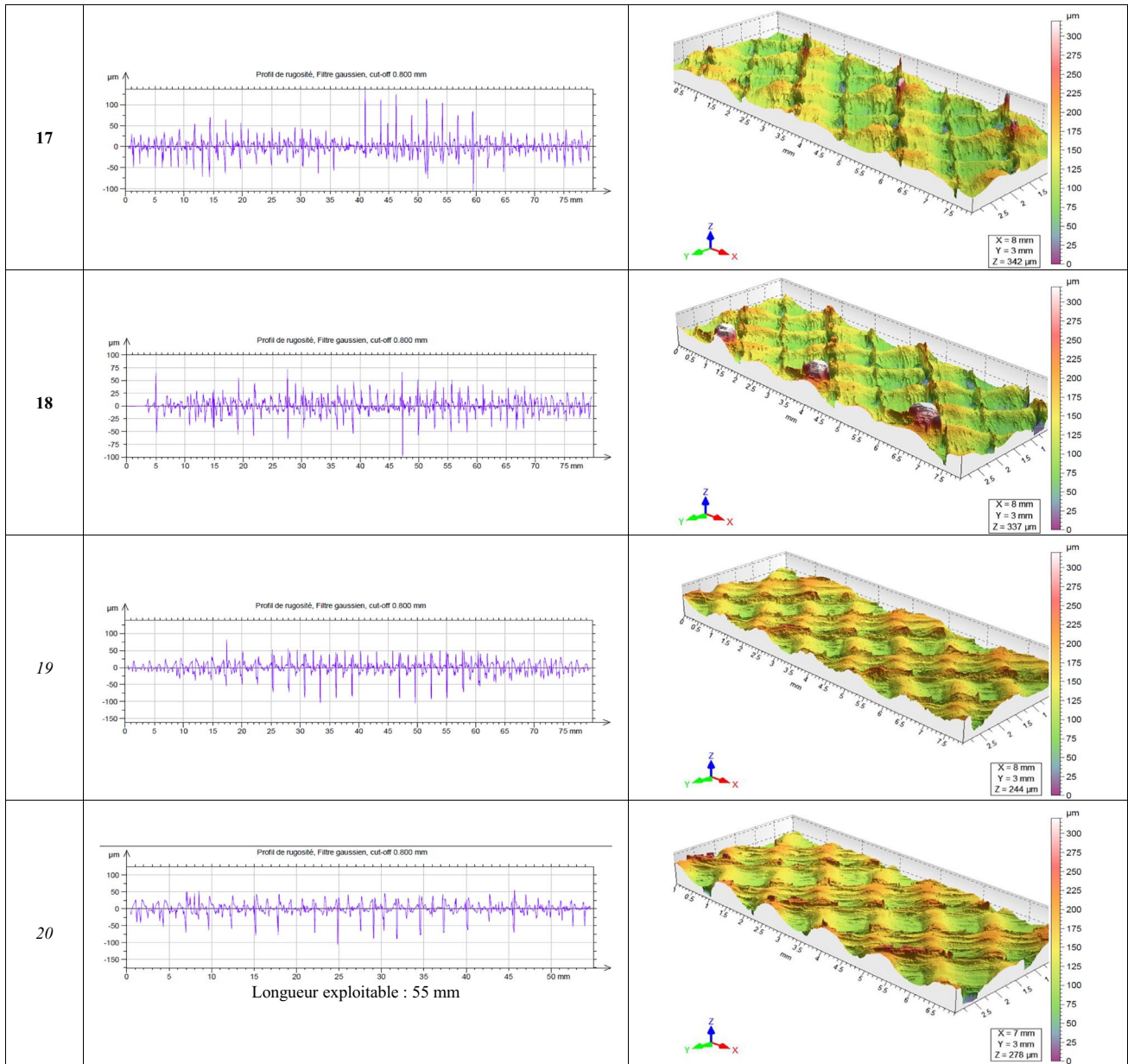
Sample's N°	2D Profile	3D Profile
1	 <p>Profil de rugosité, Filtre gaussien, cut-off 0.800 mm</p>	 <p>X = 8 mm Y = 3 mm Z = 207 µm</p>
2	 <p>Profil de rugosité, Filtre gaussien, cut-off 0.800 mm</p>	 <p>X = 8 mm Y = 3 mm Z = 261 µm</p>
3	 <p>Profil de rugosité, Filtre gaussien, cut-off 0.800 mm</p>	 <p>X = 8 mm Y = 3 mm Z = 244 µm</p>
4	 <p>Profil de rugosité, Filtre gaussien, cut-off 0.800 mm</p>	 <p>X = 8 mm Y = 3 mm Z = 206 µm</p>



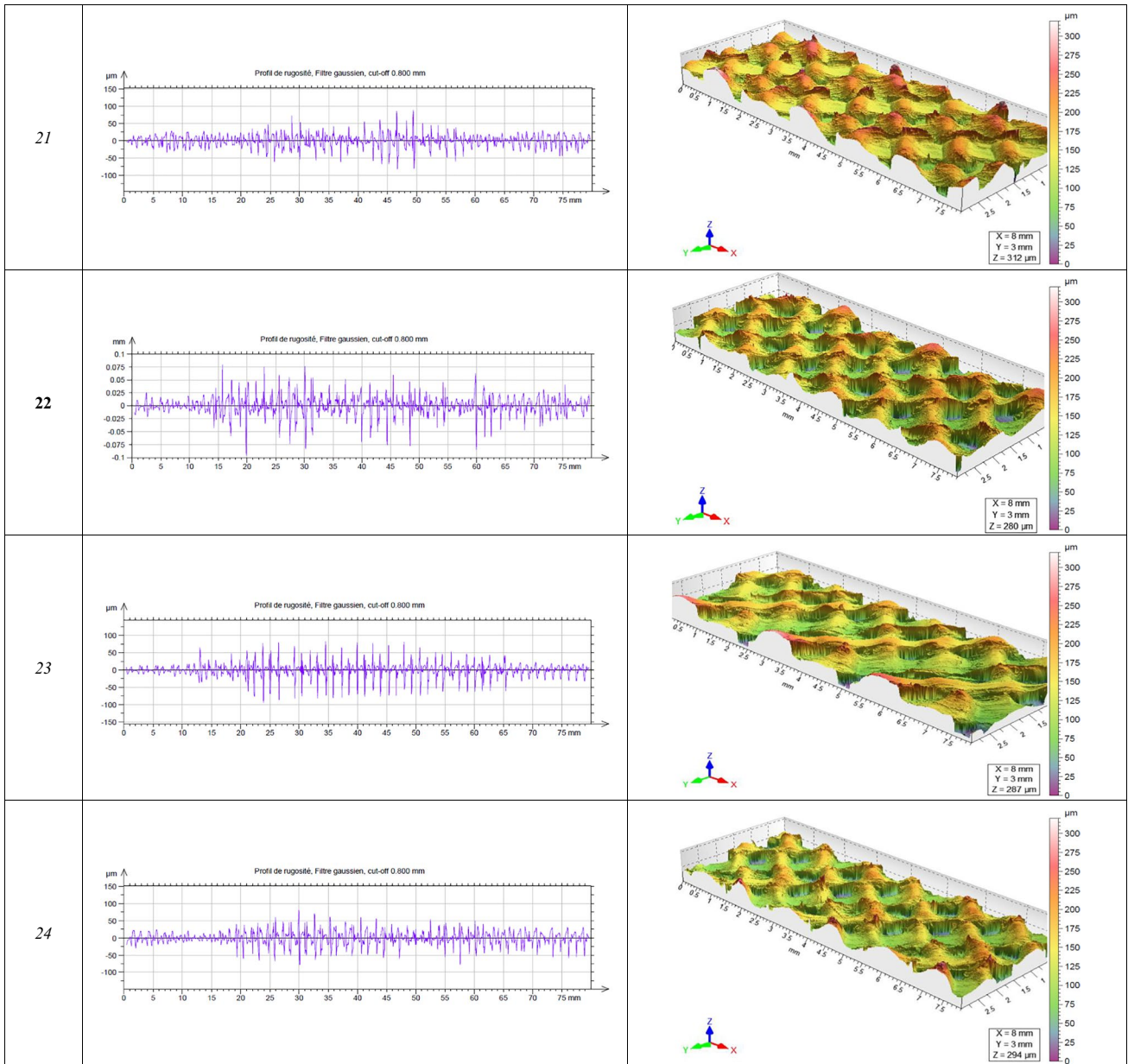




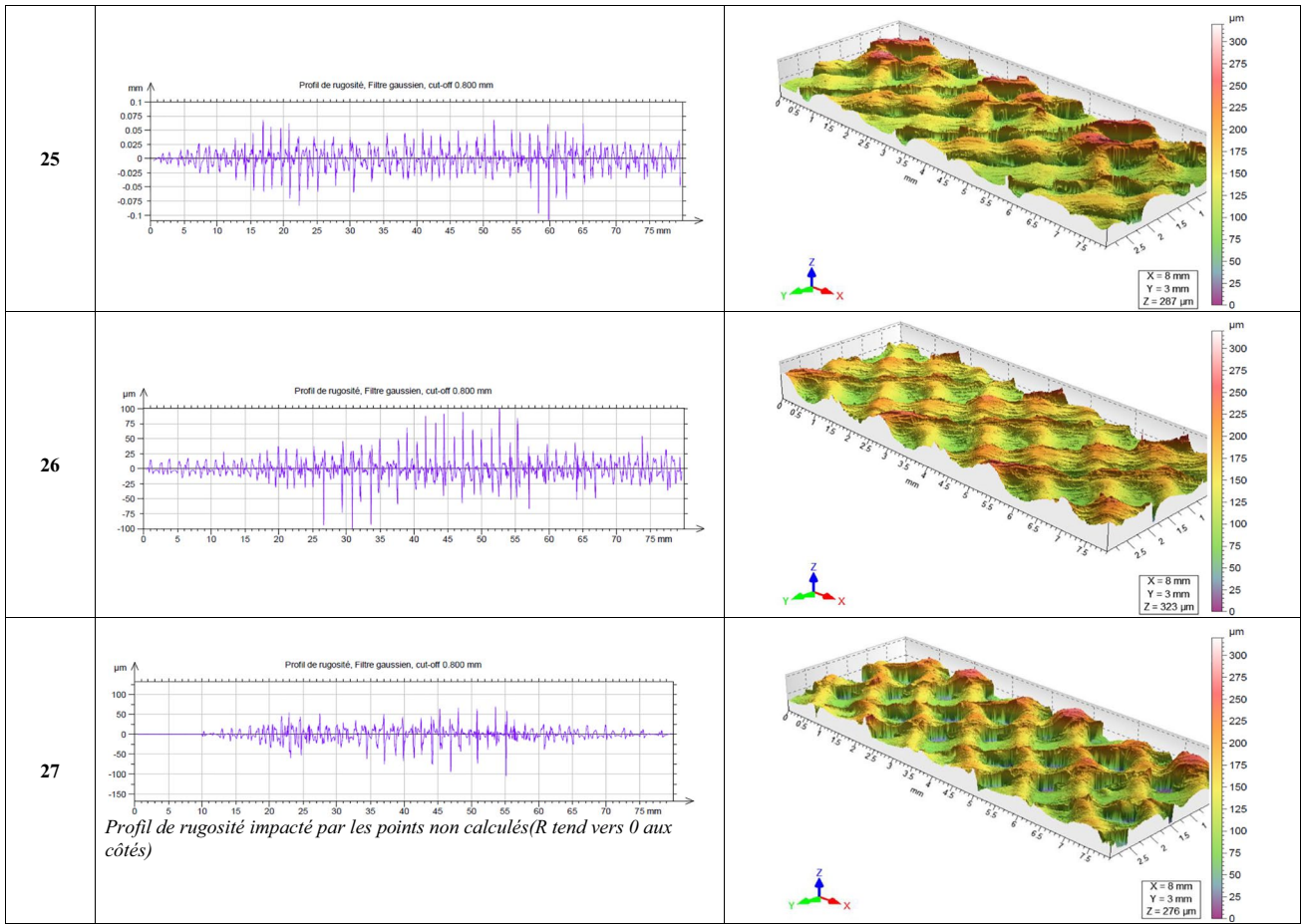












### Appendix 3. Multiway ANOVA tables and surface response (SR) plots

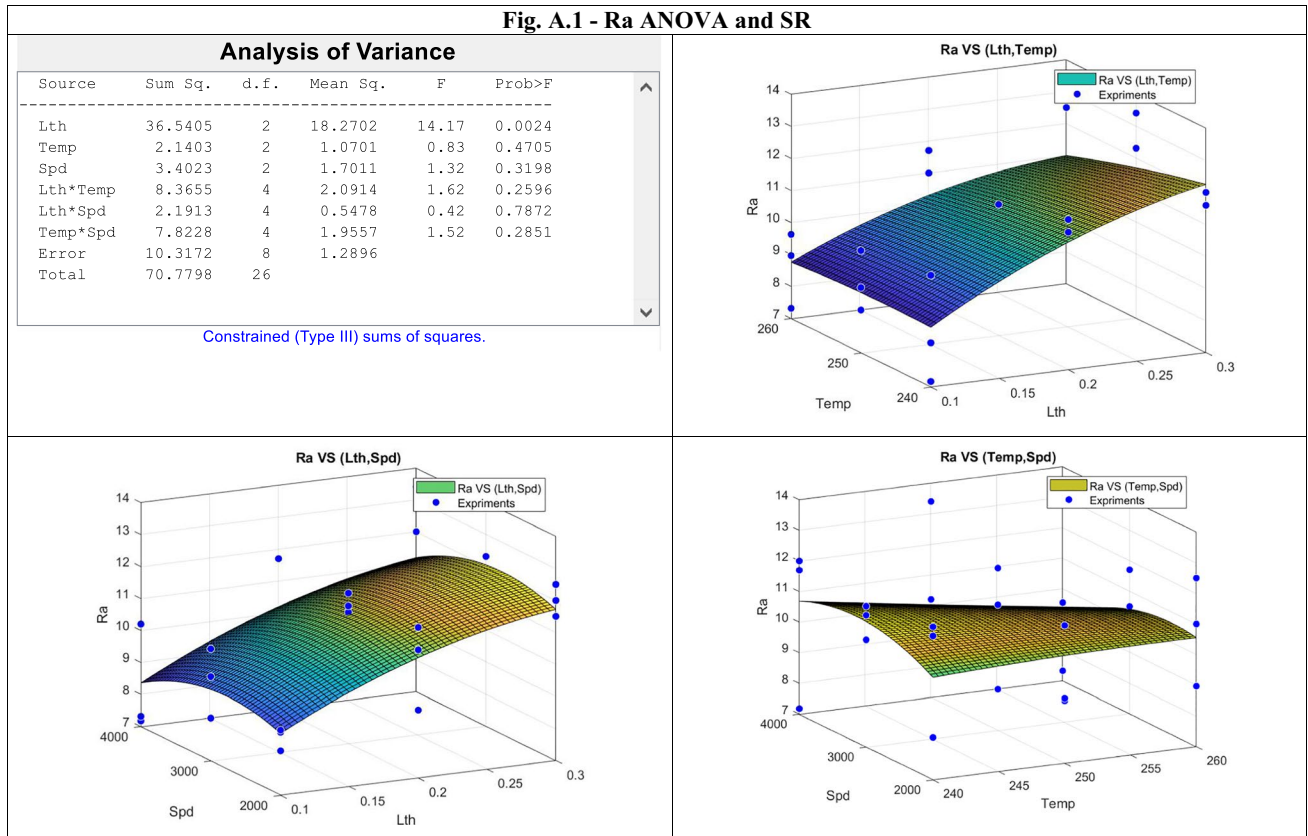


Fig. 9 Ra ANOVA and SR

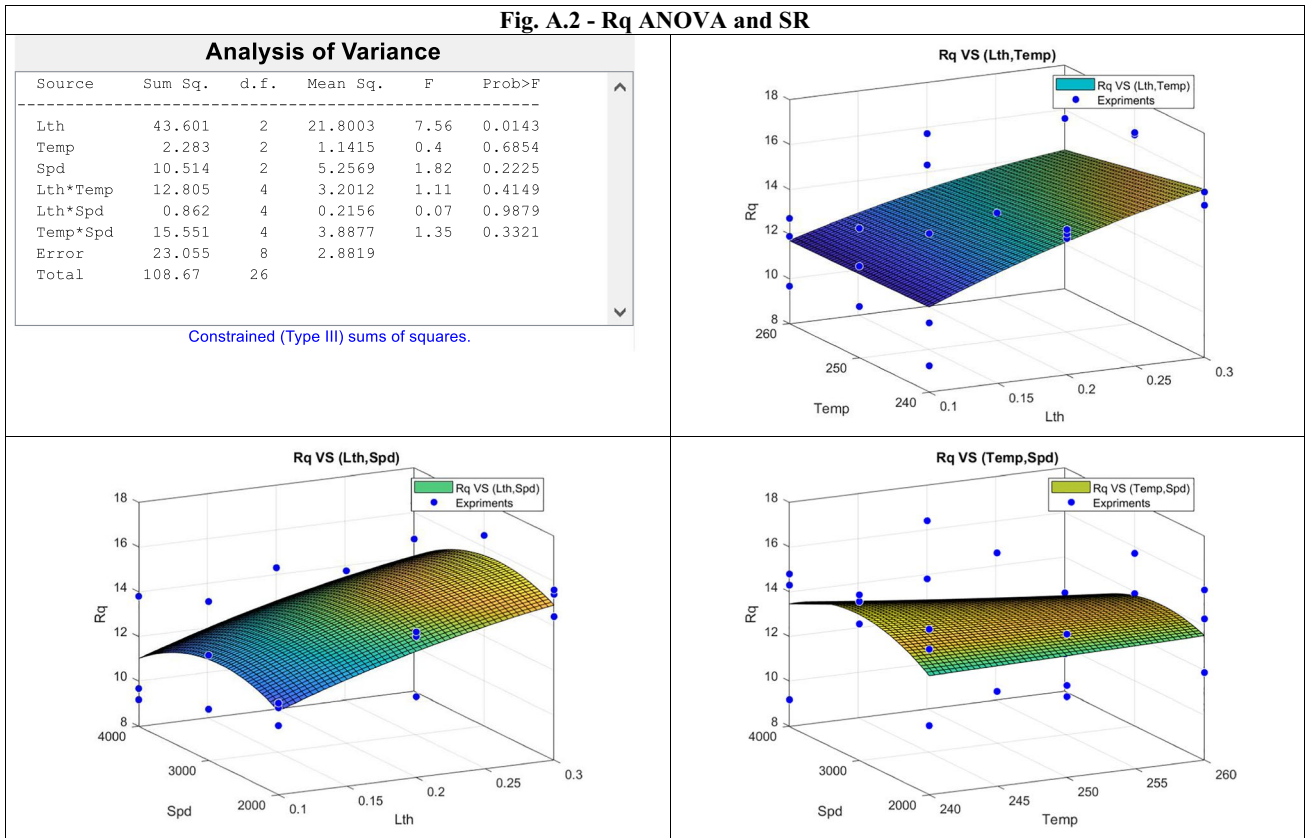


Fig. 10 Rq ANOVA and SR

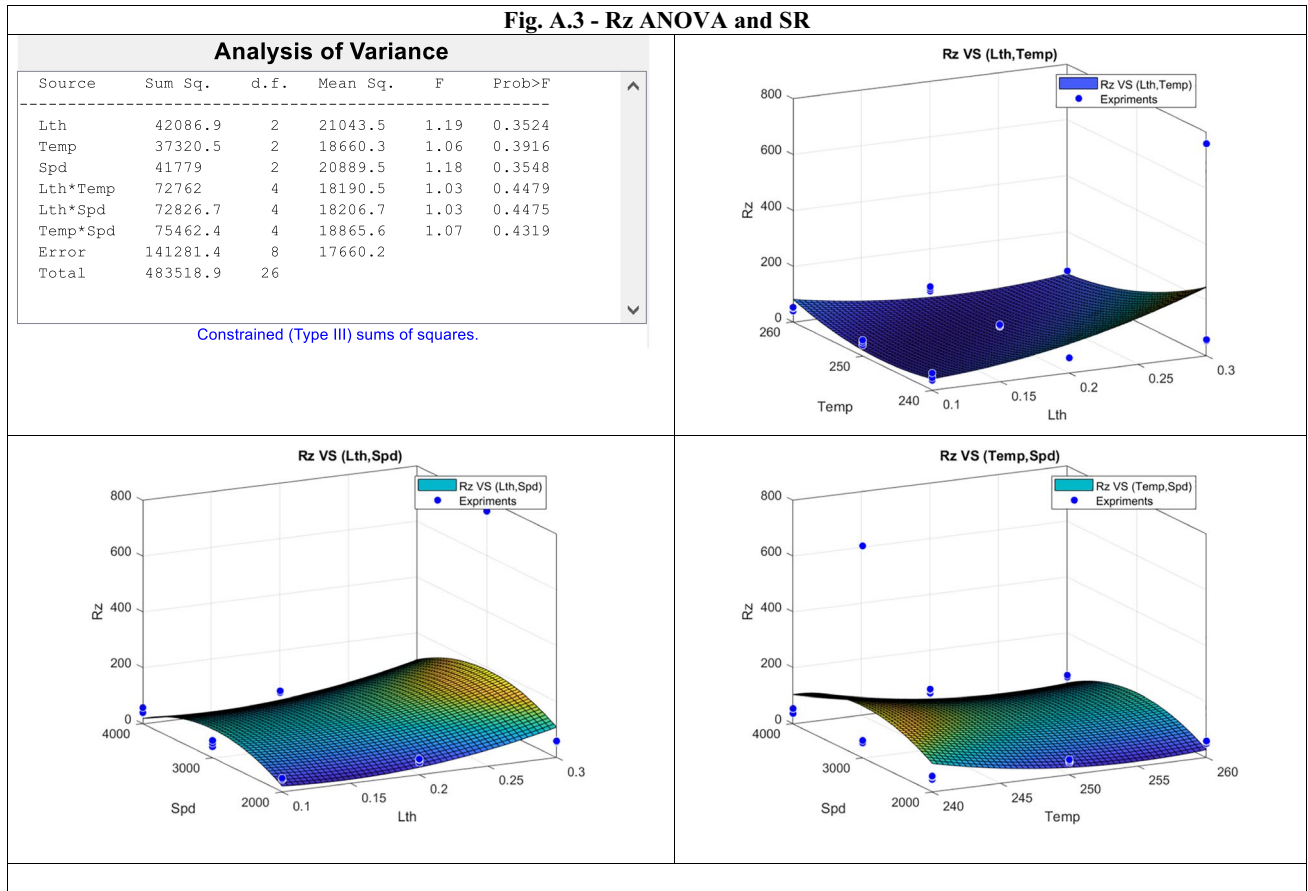


Fig. 11 Rz ANOVA and SR

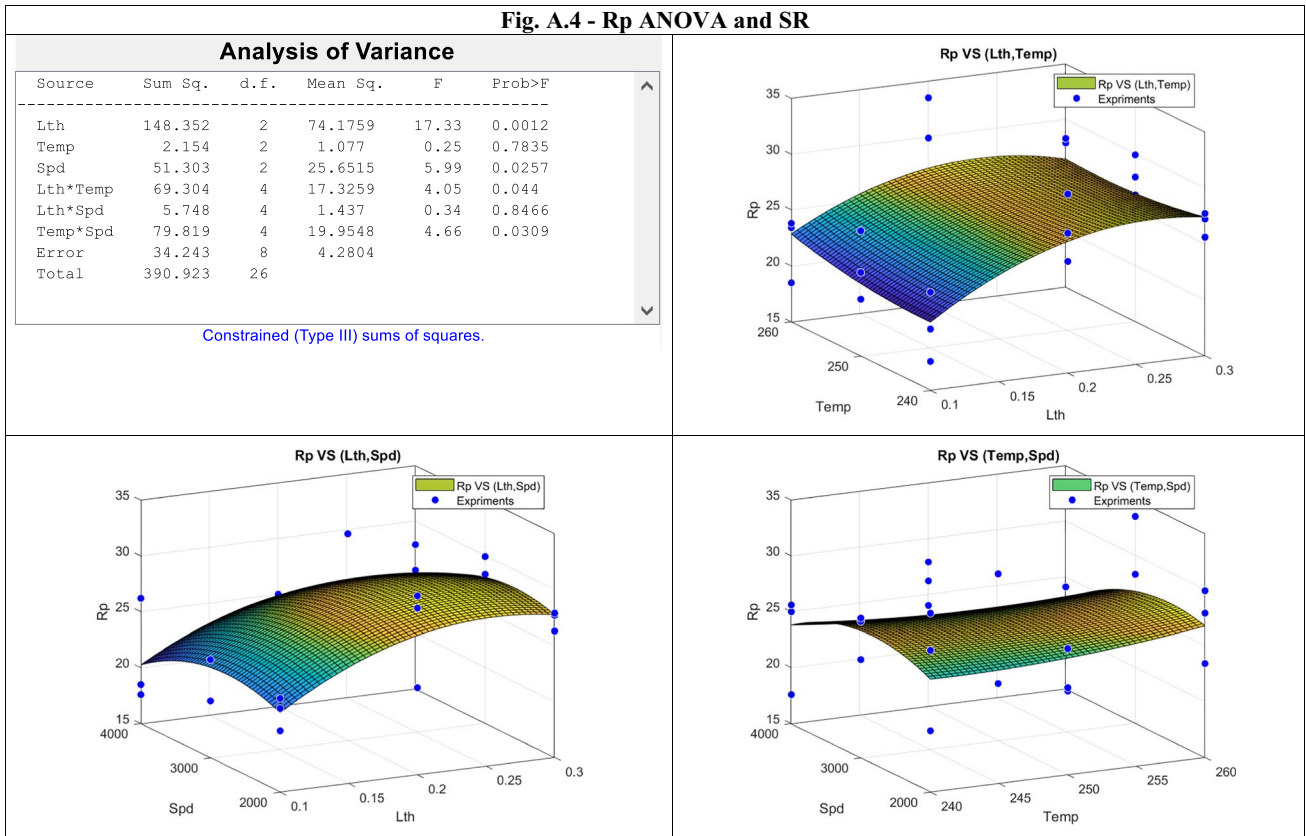


Fig. 12 Rp ANOVA and SR



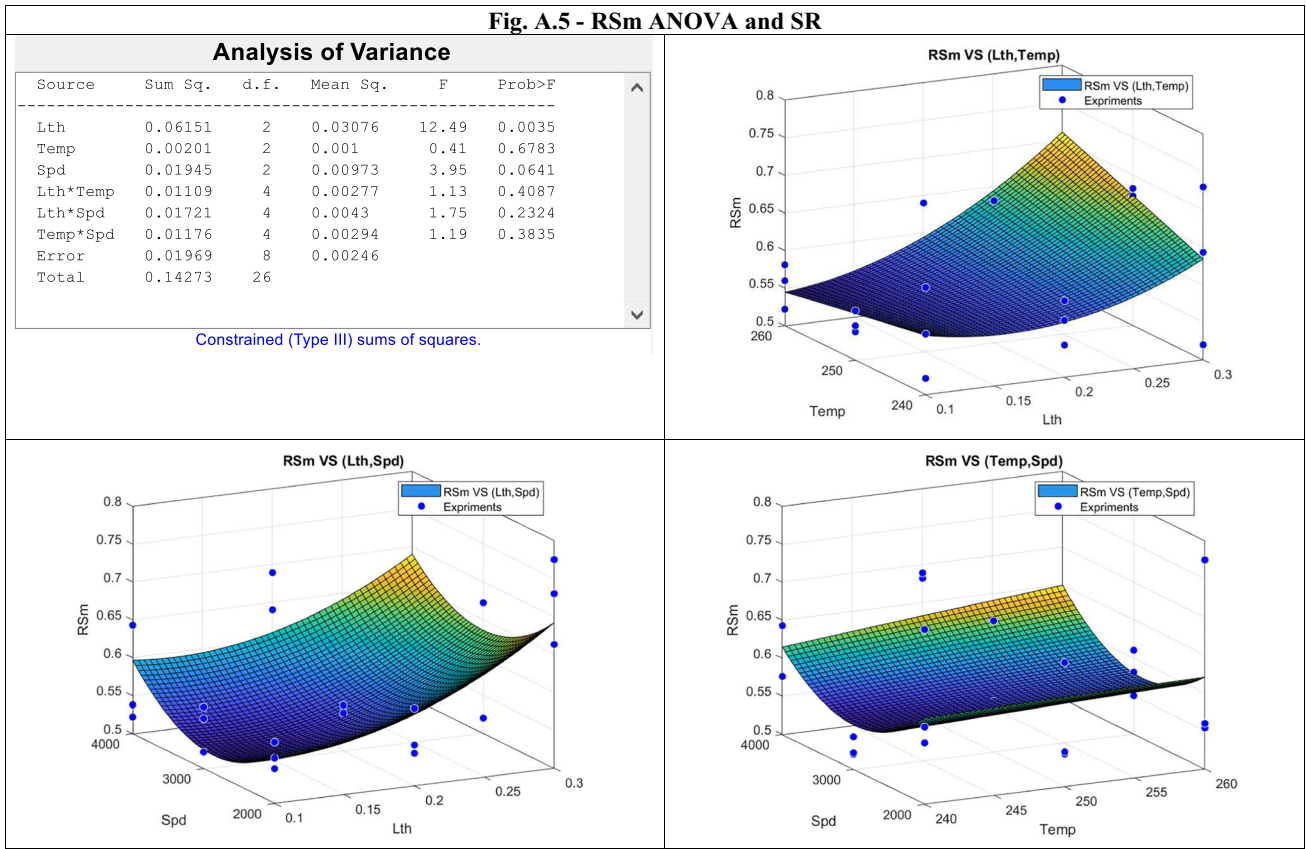


Fig. 13 RSm ANOVA and SR

### Appendix 4. Simple effects and interactions' plots

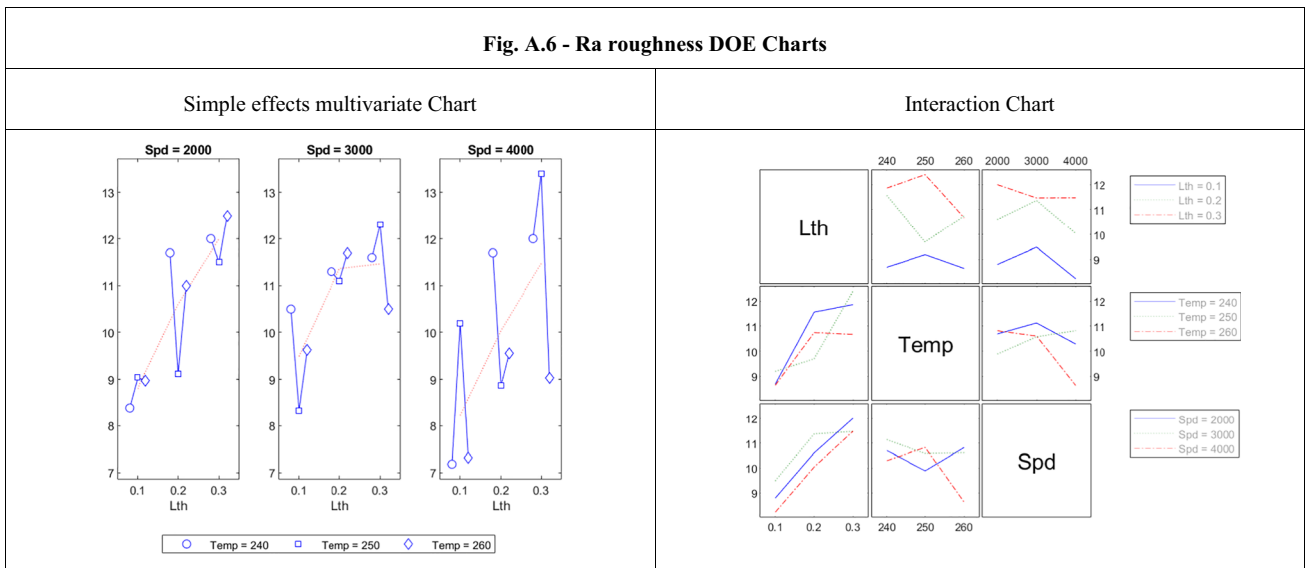


Fig. 14 Ra roughness DOE charts

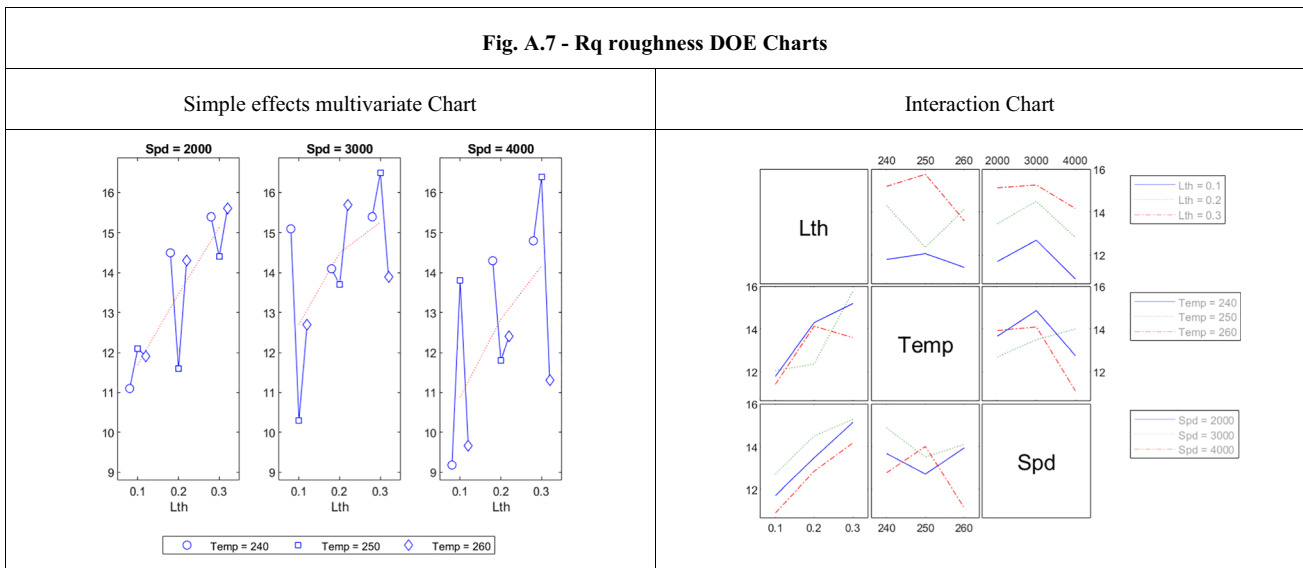


Fig. 15 Rq roughness DOE charts

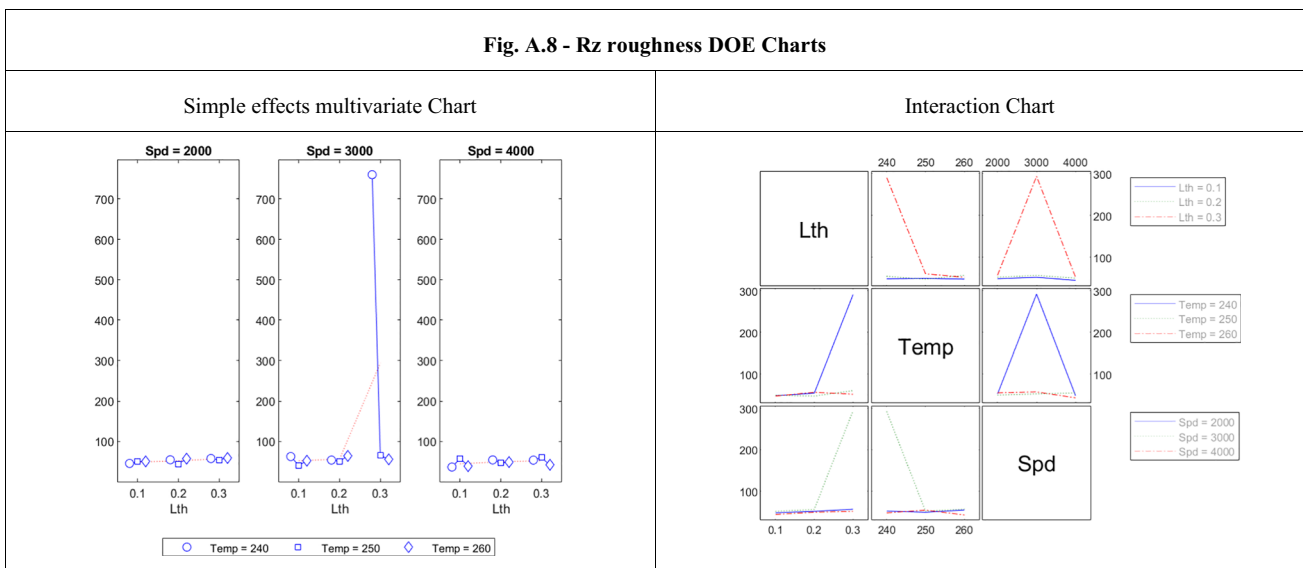


Fig. 16 Rz roughness DOE charts

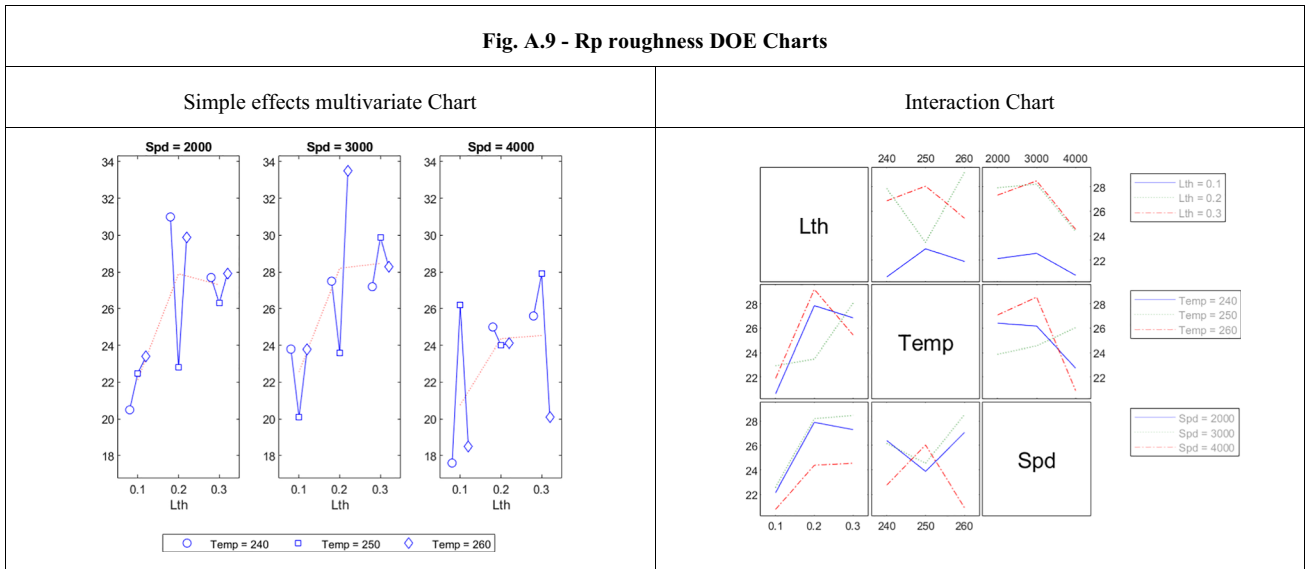


Fig. 17 Rp roughness DOE charts

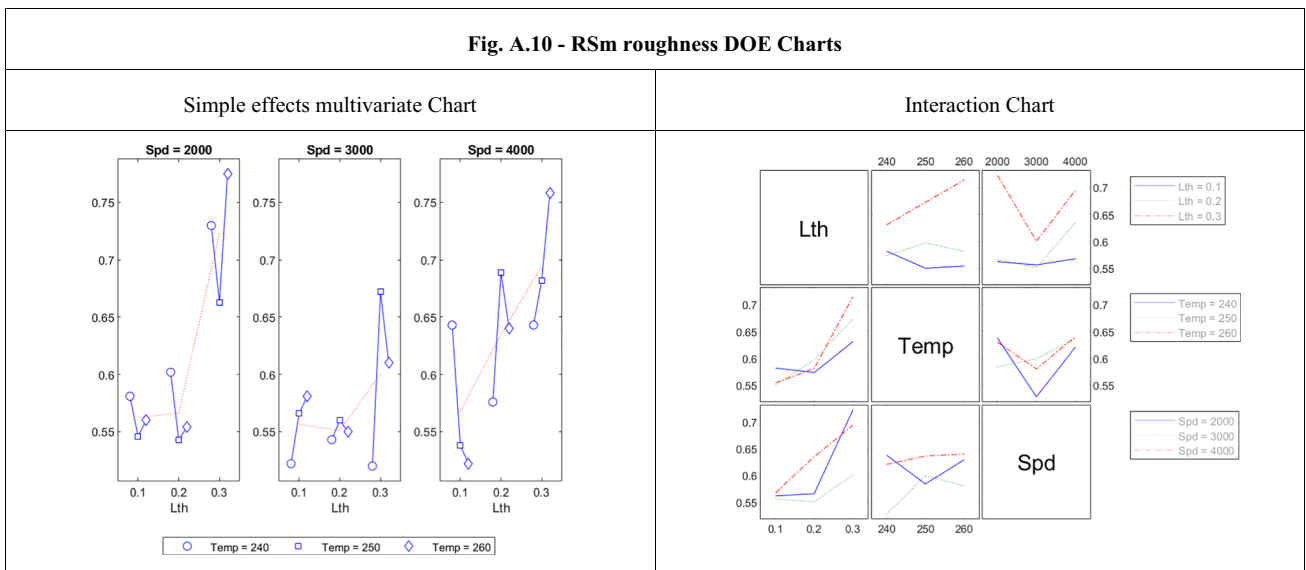


Fig. 18 RSm roughness DOE charts

**Data availability** All data required are presented in the text.

## Declarations

**Ethics approval and consent to participate** None.

**Consent for publication** None.

**Conflict of interest** The authors declare no competing interests.

## References

- Gibson I, Rosen D, Stucker B (2015) Additive manufacturing technologies: 3D printing, rapid prototyping, and direct digital manufacturing. Springer New York, New York. <https://doi.org/10.1007/978-1-4939-2113-3>
- Hopkinson N, Hague RJM, Dickens PM (eds) (2006) Rapid manufacturing: an industrial revolution for the digital age. Chichester, England: John Wiley
- Pant M, Singari RM, Arora PK, Moona G, Kumar H (2020) Wear assessment of 3-D printed parts of PLA (polylactic acid) using Taguchi design and artificial neural network (ANN) technique. Mater Res Express 7(11):115307
- Wang R-J, Wang L, Zhao L, Liu Z (2007) Influence of process parameters on part shrinkage in SLS. Int J Adv Manuf Technol 33(5–6):498–504. <https://doi.org/10.1007/s00170-006-0490-x>
- Fri K et al (2023) Microstructural and heat treatment analysis of 316L elaborated by SLM additive manufacturing process. Int J Adv Manuf Technol 124(7–8):2289–2297. <https://doi.org/10.1007/s00170-022-10622-4>
- ISO/ASTM 52900:2021 — additive manufacturing — general principles — fundamentals and vocabulary. [Online]. Available: <https://www.iso.org/standard/74514.html>. Accessed 6 Mar 2023
- Mohamed OA, Masood SH, Bhowmik JL (2015) Optimization of fused deposition modeling process parameters: a review of current research and future prospects. Adv Manuf 3(1):42–53. <https://doi.org/10.1007/s40436-014-0097-7>
- Montero M, Roundy S, Odell D, Ahn S-H, Wright PK (2001) Material characterisation of fused deposition modeling (FDM) ABS by designed experiments
- Ahn S, Montero M, Odell D, Roundy S, Wright PK (2002) Anisotropic material properties of fused deposition modeling ABS. Rapid Prototyp J 8(4):248–257. <https://doi.org/10.1108/13552540210441166>
- Fernandez-Vicente M, Calle W, Ferrandiz S, Conejero A (2016) Effect of infill parameters on tensile mechanical behavior in desktop 3D printing. 3D Print. Addit Manuf 3(3):183–192. <https://doi.org/10.1089/3dp.2015.0036>
- El Jai M, Saidou N, Zineddine M, Bachiri H (2021) Mathematical design and preliminary mechanical analysis of the new lattice structure: ‘GE-SEZ\*’ structure processed by ABS polymer and FDM technology. Prog Addit Manuf 6(1):93–118. <https://doi.org/10.1007/s40964-020-00148-0>
- Rangisetty S, Peel LD (2017) The effect of infill patterns and annealing on mechanical properties of additively manufactured thermoplastic composites. In: Volume 1: Development and characterization of multifunctional materials; mechanics and behavior of active materials; bioinspired smart materials and systems; energy harvesting; emerging technologies. Snowbird, Utah, USA, V001T08A017. <https://doi.org/10.1115/SMASIS2017-4011>
- Sood AK, Ohdar RK, Mahapatra SS (2009) Improving dimensional accuracy of fused deposition modelling processed part using grey Taguchi method. Mater Des 30(10):4243–4252. <https://doi.org/10.1016/j.matdes.2009.04.030>
- Alafaghani A, Qattawi A (2018) Investigating the effect of fused deposition modeling processing parameters using Taguchi design of experiment method. J Manuf Process 36:164–174. <https://doi.org/10.1016/j.jmapro.2018.09.025>
- Lieneke T, Denzer V, Adam GAO, Zimmer D (2016) Dimensional tolerances for additive manufacturing: experimental investigation for fused deposition modeling. Procedia CIRP 43:286–291. <https://doi.org/10.1016/j.procir.2016.02.361>
- Xu F, Wong YS, Loh HT (2000) Toward generic models for comparative evaluation and process selection in rapid prototyping and manufacturing. J Manuf Syst 19(5)
- Anitha R, Arunachalam S, Radhakrishnan P (2001) Critical parameters influencing the quality of prototypes in fused deposition modelling. J Mater Process Technol
- Byun HS, Lee KH (2006) Determination of optimal build direction in rapid prototyping with variable slicing. Int J Adv Manuf Technol 28(3–4):307. <https://doi.org/10.1007/s00170-004-2355-5>
- Saad MS, Nor AM, Baharudin ME, Zakaria MZ, Aiman AF (2019) Optimization of surface roughness in FDM 3D printer using response surface methodology, particle swarm optimization, and symbiotic organism search algorithms. Int J Adv Manuf Technol 105(12):5121–5137. <https://doi.org/10.1007/s00170-019-04568-3>
- Jee H, Sachs E (2000) Surface macro-texture design for rapid prototyping. Rapid Prototyp J 6(1):50–60. <https://doi.org/10.1108/13552540010309877>
- Lalehpour A, Janeteas C, Barari A (2018) Surface roughness of FDM parts after post-processing with acetone vapor bath smoothing process. Int J Adv Manuf Technol 95(1–4):1505–1520. <https://doi.org/10.1007/s00170-017-1165-5>
- Vahabli E, Rahmati S (2017) Hybrid estimation of surface roughness distribution in FDM parts using analytical modeling and empirical investigation. Int J Adv Manuf Technol 88(5–8):2287–2303. <https://doi.org/10.1007/s00170-016-8949-x>
- Jiang S, Hu K, Zhan Y, Zhao C, Li X (2022) Theoretical and experimental investigation on the 3D surface roughness of material extrusion additive manufacturing products. Polymers 14(2):293. <https://doi.org/10.3390/polym14020293>
- Rahmati S, Vahabli E (2015) Evaluation of analytical modeling for improvement of surface roughness of FDM test part using measurement results. Int J Adv Manuf Technol 79(5–8):823–829. <https://doi.org/10.1007/s00170-015-6879-7>
- Ouazzani K, El Jai M, Elfahime B (2022) Detailed classification of FDM (fused deposition modeling) process parameters and potentially affected part characteristics. In: 2022 2nd International Conference on Innovative Research in Applied Science, Engineering and Technology (IRASET). IRASET, Meknes, pp 1–9. <https://doi.org/10.1109/IRASET52964.2022.9738432>
- Thrimurthulu K, Pandey PM, Reddy NV (2004) Optimum part deposition orientation in fused deposition modeling. Int J Mach Tools Manuf 44(6):585–594. <https://doi.org/10.1016/j.ijmactools.2003.12.004>
- Chohan JS, Singh R (2017) Pre and post processing techniques to improve surface characteristics of FDM parts: a state of art review and future applications. Rapid Prototyp J 23(3):495–513. <https://doi.org/10.1108/RPJ-05-2015-0059>
- Moore JD (1973) Acrylonitrile-butadiene-styrene (ABS) — a review. Composites 4(3):118–130. [https://doi.org/10.1016/0010-4361\(73\)90585-5](https://doi.org/10.1016/0010-4361(73)90585-5)

29. Mercier JP, Zambelli G, Kurz W (2002) Introduction to the material science (French)- *Traité des Matériaux*, 3rd edn. Presses Polytechniques et Universitaires Romandes, Lausanne
30. Carrega M, Verney V (2017) *Plastic materials (French)*, 4th edn. Dunod, Malakoff
31. Alkhuder A (2014) Structuration des mélanges ABS/PC en vue du recyclage des DEEE. Conservatoire national des arts et métiers - CNAM. [Online]. Available: <https://theses.hal.science/tel-01132493>
32. Wypych G (2012) *Handbook of polymers*. ChemTec Edition
33. "Stratasys ABS-M30 Datasheet -FDM Thermoplastic Filament-." Accessed: Mar. 07, 2023. [Online]. Available: [https://www.stratasys.com/siteassets/materials/materials-catalog/fdm-materials/abs-m30/mds\\_fdm\\_abs-m30\\_0921a.pdf](https://www.stratasys.com/siteassets/materials/materials-catalog/fdm-materials/abs-m30/mds_fdm_abs-m30_0921a.pdf)
34. Ananthapadmanabha GS, Deshpande VV (2016) Thermal properties of acrylonitrile butadiene styrene composites. *Indian J Adv Chem Sci* 1:279–282
35. Praveen RN, Muruli D, Sandesh SN (2013) Tribological characteristics of acrylonitrile-butadiene-styrene (ABS) thermoplastic composites. *Int J Mech Eng Robot Res* 2(4)
36. Wilkes CE, Summers JW, Daniels CA, Berard MT (eds) (2005) Hanser, Munich; Cincinnati
37. Torrado Perez AR, Roberson DA, Wicker RB (2014) Fracture surface analysis of 3D-printed tensile specimens of novel ABS-based materials. *J. Fail. Anal. Prev* 14(3):343–353. <https://doi.org/10.1007/s11668-014-9803-9>
38. Weng Z, Wang J, Senthil T, Wu L (2016) Mechanical and thermal properties of ABS/montmorillonite nanocomposites for fused deposition modeling 3D printing. *Mater Des* 102:276–283. <https://doi.org/10.1016/j.matdes.2016.04.045>
39. Romanova N, Shafigullin L, Gabdrakhmanov A, Buyatova S (2019) Thermal properties of products based on ABS/PC. In: MATEC Web of Conferences 298:00016. <https://doi.org/10.1051/mateconf/201929800016>
40. Kumar V, Singh R, Ahuja IPS (2020) On mechanical and thermal properties of cryo-milled primary recycled ABS. *Sādhanā* 45(1):80. <https://doi.org/10.1007/s12046-020-1317-4>
41. Lyon RE, Janssens ML (2005) *Polymer flammability*. Office of Aviation Research, Washington, DC
42. Rahman M, Schott NR, Sadhu LK (2016) Glass transition of ABS in 3D printing. In: *Proceedings of 2016 COMSOL Conference*. COMSOL, Boston
43. Song B (2022) Study on dielectric and thermal properties of ABS/multilayer graphene composites. *J Phys Conf Ser* 2247(1):012011. <https://doi.org/10.1088/1742-6596/2247/1/012011>
44. Mondal A, Sohel MdA, Arif PM, Thomas S, SenGupta A (2021) Effect of ABS on non-isothermal crystallization kinetics of polyamide 6. *J Therm Anal Calorim* 146:2489–2501
45. Selvamani SK et al (2019) 3D printing: overview of ABS evolution. In: *Proceedings of the 3rd International Conference on Automotive Innovation Green Energy Vehicle*. AIP, Kuantan, p 020041. <https://doi.org/10.1063/1.5085984>
46. Amendola C et al (2021) Optical characterization of 3D printed PLA and ABS filaments for diffuse optics applications. *PLOS ONE* 16(6):e0253181. <https://doi.org/10.1371/journal.pone.0253181>
47. Salman SR, Al-Shama'a ND (1991) Effect of thermal aging on the optical properties of ABS plastics. *Polym-Plast Technol Eng* 30(4):343–349. <https://doi.org/10.1080/03602559108021000>
48. Ferreira SLC et al (2007) Box-Behnken design: an alternative for the optimization of analytical methods. *Anal Chim Acta* 597(2):179–186. <https://doi.org/10.1016/j.aca.2007.07.011>
49. Soffie SM, Ismail I, Nurain MA, Aqida SN (2020) The morphological and surface roughness of magnetorheological polished AISI 6010 surface
50. Rajesh N, Guru Mahesh G, Venkataramaiah P (2022) Study of machining parameters on tensile strength and surface roughness of ABS samples printed by FDM. *Adv Mater Process Technol* 8:1373–1385. <https://doi.org/10.1080/2374068X.2021.1946758>
51. Roy RK (2010) *A primer on the Taguchi method*, 2nd edn. Society of Manufacturing Engineers, Dearborn, Mich
52. *Explanation of surface characteristics—standards*. Accretech-Tokyo Seimitsu. [Online]. Available: <https://inspectionengineering.com/wp-content/uploads/2018/03/SurfaceFinishExplains.pdf>
53. Gadelmawla ES, Koura MM, Maksoud TMA, Elewa IM, Soliman HH (2002) Roughness parameters. *J Mater Process Technol* 123(1):133–145. [https://doi.org/10.1016/S0924-0136\(02\)00060-2](https://doi.org/10.1016/S0924-0136(02)00060-2)
54. Kattethota G, Henderson M (1998) A visual tool to improve layered manufacturing part quality
55. Badola M, Vaishya RO (2016) Parameters affecting surface roughness of fused deposition modeling. *Manag J Mech Eng* 6(1):34. <https://doi.org/10.26634/jme.6.1.3739>
56. Chohan JS et al (2022) Optimization of FDM printing process parameters on surface finish, thickness, and outer dimension with ABS polymer specimens using Taguchi orthogonal array and genetic algorithms. *Math Probl Eng* 2022:1–13. <https://doi.org/10.1155/2022/2698845>
57. Pérez M, Medina-Sánchez G, García-Collado A, Gupta M, Carou D (2018) Surface quality enhancement of fused deposition modeling (FDM) printed samples based on the selection of critical printing parameters. *Materials* 11(8):1382. <https://doi.org/10.3390/ma11081382>
58. Hall DC, Palmer P, Ji H-F, Ehrlich GD, Król JE (2021) Bacterial biofilm growth on 3D-printed materials. *Front Microbiol* 12:646303. <https://doi.org/10.3389/fmicb.2021.646303>
59. Han W, Jafari MA, Danforth SC, Safari A (2002) Tool path-based deposition planning in fused deposition processes. *J Manuf Sci Eng* 124(2):462–472. <https://doi.org/10.1115/1.1455026>
60. EhsanulHaque M, Banerjee D, Bikash Mishra S, Kumar Nanda B (2019) A numerical approach to measure the surface roughness of FDM build part. *Mater Today Proc* 18:5523–5529. <https://doi.org/10.1016/j.matpr.2019.07.659>

**Publisher's Note** Springer Nature remains neutral with regard to jurisdictional claims in published maps and institutional affiliations.

Springer Nature or its licensor (e.g. a society or other partner) holds exclusive rights to this article under a publishing agreement with the author(s) or other rightsholder(s); author self-archiving of the accepted manuscript version of this article is solely governed by the terms of such publishing agreement and applicable law.